Universidad de Investigación de Tecnología Experimental Yachay

Escuela de Ciencias Químicas e Ingeniería

TITULO: Theoretical study on the Photoactivated anticancer drugs based on platinum coordination compounds.

Trabajo de integración curricular presentado como requisito para la obtención de título como Química

Autor:

Paula Gabriela Cárdenas Cárdenas

Tutor:

Juan Pablo Saucedo, PhD.

Co-tutor:

Thibault Terencio, PhD.

Urcuquí, September 2020

UNIVERSIDAD YACHAY TECH

Urcuquí, 5 de noviembre de 2020

SECRETARÍA GENERAL
(Vicerrectorado Académico/Cancillería)
ESCUELA DE CIENCIAS QUÍMICAS E INGENIERÍA
CARRERA DE QUÍMICA
ACTA DE DEFENSA No. UITEY-CHE-2020-00061-AD

A los 5 días del mes de noviembre de 2020, a las 15:00 horas, de manera virtual mediante videoconferencia, y ante el Tribunal Calificador, integrado por los docentes:

Presidente Tribunal de Defensa	Dr. CAETANO SOUSA MANUEL , Ph.D.
Miembro No Tutor	Dr. OROPEZA OREA, RUTH FIDELINA , Ph.D.
Tutor	Dr. SAUCEDO VAZQUEZ, JUAN PABLO , Ph.D.

El(la) señor(ita) estudiante **CARDENAS CARDENAS, PAULA GABRIELA**, con cédula de identidad No. **0105295109**, de la **ESCUELA DE CIENCIAS QUÍMICAS E INGENIERÍA**, de la Carrera de **QUÍMICA**, aprobada por el Consejo de Educación Superior (CES), mediante Resolución **RPC-SO-39-No.456-2014**, realiza a través de videoconferencia, la sustentación de su trabajo de titulación denominado: **THEORETICAL STUDY ON THE PHOTOACTIVATED ANTICANCER DRUGS BASED ON PLATINUM COORDINATION COMPOUNDS**, previa a la obtención del título de **QUÍMICO/A**.

El citado trabajo de titulación, fue debidamente aprobado por el(los) docente(s):

Tutor	Dr. SAUCEDO VAZQUEZ, JUAN PABLO , Ph.D.
Co - Tutor	Dr. TERENCIO THIBAULT , Ph.D.

Y recibió las observaciones de los otros miembros del Tribunal Calificador, las mismas que han sido incorporadas por el(la) estudiante.

Previamente cumplidos los requisitos legales y reglamentarios, el trabajo de titulación fue sustentado por el(la) estudiante y examinado por los miembros del Tribunal Calificador. Escuchada la sustentación del trabajo de titulación a través de videoconferencia, que integró la exposición de el(la) estudiante sobre el contenido de la misma y las preguntas formuladas por los miembros del Tribunal, se califica la sustentación del trabajo de titulación con las siguientes calificaciones:

Tipo	Docente	Calificación
Miembro Tribunal De Defensa	Dr. OROPEZA OREA, RUTH FIDELINA , Ph.D.	10,0
Tutor	Dr. SAUCEDO VAZQUEZ, JUAN PABLO , Ph.D.	10,0
Presidente Tribunal De Defensa	Dr. CAETANO SOUSA MANUEL , Ph.D.	9,5

Lo que da un promedio de: **9.8 (Nueve punto Ocho)**, sobre 10 (diez), equivalente a: **APROBADO**

Para constancia de lo actuado, firman los miembros del Tribunal Calificador, el/la estudiante y el/la secretario ad-hoc.

Certifico que *en cumplimiento del Decreto Ejecutivo 1017 de 16 de marzo de 2020, la defensa de trabajo de titulación (o examen de grado modalidad teórico práctica) se realizó vía virtual, por lo que las firmas de los miembros del Tribunal de Defensa de Grado, constan en forma digital.*

CARDENAS CARDENAS, PAULA GABRIELA
Estudiante

Dr. CAETANO SOUSA MANUEL , Ph.D.
Presidente Tribunal de Defensa

MANUEL CAETANO SOUSA
Digitally signed by MANUEL CAETANO SOUSA
Date: 2020.11.05 19:23:14 -05'00'

Dr. SAUCEDO VAZQUEZ, JUAN PABLO , Ph.D.
Tutor

JUAN PABLO
SAUCEDO
VAZQUEZ

Firmado digitalmente por JUAN PABLO
SAUCEDO VAZQUEZ
Nombre de reconocimiento (DN): c=EC,
o=BANCO CENTRAL DEL ECUADOR,
ou=ENTIDAD DE CERTIFICACION DE
INFORMACION-ECIBCE, l=QUITO,
serialNumber=0000268799, cn=JUAN
PABLO SAUCEDO VAZQUEZ
Fecha: 2020.11.05 20:48:58 -05'00'

Dr. OROPEZA OREA, RUTH FIDELINA , Ph.D.
Miembro No Tutor

RUTH FIDELINA
OROPEZA OREA

Firmado digitalmente por
RUTH FIDELINA OROPEZA
OREA
Fecha: 2020.11.05 21:21:02
-05'00'

CIFUENTES TAFUR, EVELYN CAROLINA
Secretario Ad-hoc

Firmado electrónicamente por:
EVELYN CAROLINA
CIFUENTES TAFUR

AUTORÍA

Yo, **PAULA GABRIELA CARDENAS CARDENAS**, con cédula de identidad 0105295109, declaro que las ideas, juicios, valoraciones, interpretaciones, consultas bibliográficas, definiciones y conceptualizaciones expuestas en el presente trabajo; así cómo, los procedimientos y herramientas utilizadas en la investigación, son de absoluta responsabilidad de el/la autora (a) del trabajo de integración curricular, ensayo o artículo científico. Así mismo, me acojo a los reglamentos internos de la Universidad de Investigación de Tecnología Experimental Yachay.

Urcuquí, Septiembre 2020.

_____

Paula Gabriela Cárdenas Cárdenas

CI: 0105295109

AUTORIZACIÓN DE PUBLICACIÓN

Yo, **PAULA GABRIELA CARDENAS CARDENAS**, con cédula de identidad 0105295109, cedo a la Universidad de Tecnología Experimental Yachay, los derechos de publicación de la presente obra, sin que deba haber un reconocimiento económico por este concepto.

Asimismo, autorizo a la Universidad que realice la digitalización y publicación de este trabajo de integración curricular, en el repositorio virtual, de conformidad a lo dispuesto en el Art. 144 de la Ley Orgánica de Educación Superior. En caso que el ensayo o artículo se encuentre aprobado para publicación en bases indexadas, únicamente se publicará el resumen del mismo.

Urcuquí, Septiembre 2020.

Paula Gabriela Cárdenas Cárdenas

CI: 0105295109

DEDICATORIA

A mis padres,

A mi Sol y a mi Oso,

A mis amigos,

A todos mis seres amados.

AGRADECIMIENTO

A mis padres, Sara y Edgar, por haberme apoyado todo el tiempo. A mis amigos que se convirtieron en mi familia, en especial a Cindhy, Eli y May. A mis profesores, de manera especial a Juan Pablo y a Thibu por haberme enseñado tanto. A mi familia.

Resumen

El cáncer es la segunda causa principal de muerte a nivel mundial. Diferentes tratamientos como quimioterapia, cirugía o radioterapia se han centrado en nuevos enfoques para un tratamiento más específico y eficaz. No fue hasta 1978 que la tasa de curación del cáncer con cisplatino atrajo el interés de compuestos a base de metales como agentes anticancerígenos. Con el tiempo, se han propuesto nuevas generaciones de diferentes compuestos que contienen metales con citotoxicidad mejorada, con el objetivo de ser tan efectivos como el cisplatino. Con el tiempo, el cisplatino ha presentado algunos obstáculos como la resistencia al tratamiento y su falta de tratamiento dirigido. La nueva generación de fármacos fotoactivados a base de platino conduce a un nuevo enfoque que presenta un tratamiento dirigido, evitando desarrollar resistencia contra él. En este trabajo se estudiaron cuatro complejos prometedores que presentan características comunes en los ligantes para comprender mejor su comportamiento observado como longitud de onda responsable de su fototoxicidad, influencia de la orientación de los ligantes, posibilidad de acoplamiento spin orbita (SOC) y resultados de su interacción con ADN. Con el fin de obtener estos resultados, la contribución de spin orbita se calculó entre estados excitados obtenidos de la teoría funcional de la densidad dependiente del tiempo (TDDFT), teniendo como base a su geometría de singulete optimizada. Con el fin de comparar se obtuvieron geometrías de estados tripletes optimizadas. Los cálculos de TDDFT se llevaron a cabo para complejos libre de azida para conocer su geometría antes de la interacción con ADN. Para la preparación de la muestra para AutoDock, se calcularon las cargas parciales en cada átomo del complejo, esto se realizó en un proceso de dos pasos, basándonos en un blind AutoDock para lograr resultados más precisos. Finalmente, parte de la evaluación de la interacción del ADN y el complejo se llevaron a cabo en un cálculo molecular cuántico (QM) para lograr un mínimo de energía y obtener la mayor interacción posible.

Palabras clave: Fotoactivacion, Back bonding, AutoDock, Spin Orbit Coupling, Docking.

Abstract

Cancer is the second leading cause of death globally. Different treatment as chemotherapy, surgery or radiotherapy has been focusing on newly approaches to a more targeted and effective treatment. It was not until 1978 that rate of cancer healing whit cisplatin has attracted interest of metal based compounds as anticancer agents. Over time newly generations of different metal containing compound with enhanced cytotoxicity has been proposed, aiming to be as effective as cisplatin. Approved metal based drugs present some obstacles as treatment resistance and its lack of target treatment. New generation of platinum photoactivated drugs leads to a new approach presenting a target treatment and non-resistance developed against it. Four promising complexes, presenting common features in ligands will be studied to a better understanding of its observed behavior as wavelength responsible of its phototocicity, influence of ligands orientation, possibility of spin orbit coupling (SOC) for compounds and docking results with DNA. Aiming these results, SOC contribution was calculated in a time depended density functional theory (TDDFT) excited states computation based on its singlet optimization geometry. For comparison also triplet states of each geometry was obtained. TDDFT calculations were carried out for each complex with the absence of azide in order to know the geometry before DNA docking. To prepare the sample for AutoDock, partial charges on each atom in complex was calculated. AutoDock is a two steps process based on blind AutoDock to achieve a more accurate results. Finally, part of DNA and complex were carried on in a quantum molecular (QM) computation to achieve a minimum of energy and obtain more possible interaction.

Key words: Photoactivated, Back bonding, Autodock, Spin Orbit Coupling, Docking.

CONTENT

LIST OF FIGURES

Chapter I   Introduction

I.1   Introduction

Cancer has become a disease that ranks as the second leading cause of death worldwide. In 2018, 9.6 million deaths from cancer were reported in the world, the most common types were: lung, colorectal, stomach, liver and breast cancer.[1] From a deeper perspective, cancer can be defined as an abnormal cell growing beyond their usual boundaries that in some cases metastasize, causing problems on the body where it started. [2] Different factors can be related to cancer appearances such as the genetic factor of each individual, external agents, and age. When referred to external agents, these can be divided as biological carcinogens as infections, chemical as arsenic in water, and physical as UV light. Another fundamental factor is age, concomitant with a decrease in cell repairing ability. About 30-50% of the cancer burden has the possibility of being reduced by avoiding the aforementioned factors. Cancer high mortality could be avoided by early detection, allowing so an adequate and effective treatment.[1]

Cancer is an ancient sickness and logically also its treatment and the continue evolution of it. Some of the first evidence of human bone cancer was found in ancient Egypt around 1600 B.C., where it was evidenced that the only treatment used was a palliative treatment.[3] Nowadays, the most commonly used methods to treat cancer are chemotherapy, surgery, and radiotherapy that are in continuous evolution. Chemotherapy began to be used in the early 20th century, with the use of mustard gas as an alkylating agent to treat cancer. In the following years, other alkylating drugs were synthesized to treat cancer. Monotherapy drugs only show results in some types of cancer. As a consequence, adjuvant chemotherapy was used since 1960s, referring to the treatment of chemotherapy with another tumor treatment as surgery or radiotherapy.[4]

In 1978, higher cure rates were achieved using cisplatin, which was synthesized for the first time by Barnett Rosenberg in 1960.[4, 5] After this, a modern era of the metal-based anticancer drugs as carboplatin, oxaliplatin, among others started. The growing demand on the synthesis of new metal-based compounds is due to the extent and level of cytotoxicity of these compounds, and the developing resistance to anticancer drugs. Ligand substitution and modification of preexisting compounds lead to a new and wide range of them, showing different cytotoxicity and efficiency. Furthermore, one of the main goals is to determine the balance between the therapeutic and toxic doses, and also the level of toxicity, selectivity, and activity spectrum of complexes.[5]

To achieve a better selectivity, photo-activated chemotherapy has become a valuable opportunity to gain the control of when and where the anticancer drug must be activated. This is possible due to the potential of d-block metals to be excited by light, namely photoexcitation and different decay pathways, which can result in radiative energy, loss of ligands, or a transfer of energy to other species. Metal species can be easily excited by irradiation UVA and visible light.[6]

Metal complexes with d^3 and d^6 electronic configurations are the most promising ones due to their photophysical properties and their relative non-lability characteristic. Photochemical reactions as ligand dissociation or redox reactions occur at any time while system decay to the ground state. The photochemical process is not only dependent on the excited state of the molecule, but it also depends of the closely-lying states and the availability of the process previously mentioned. Depending on the molecule region most affected, excited state of metal complexes can be composed of different type of transitions as Metal-centred (MC), Charge-transfer (CT) or a Ligand-centred (LC) transition.[6]

Since the impact that platinum (Pt) complexes had on chemotherapy, the research on platinum-based compounds has increased, resulting in a family of octahedral photoactivated $Pt^{(IV)}$ complexes. The main purpose of these complexes is to become active by reduction to $Pt^{(II)}$ after light irradiation. Octahedral $Pt^{(IV)}$ complexes present a general structure in which the equatorial positions are occupied by two non-leaving ligands (in most cases amine derived ligands) and two leaving groups, and two axial ligands. The latter introduced ligands display a saturated coordination sphere avoiding an easy ligand substitution and establishing a close relationship with complex properties as lipophilicity, targeting, redox potential, among other indispensable qualities.[7] Most studied photo-activated complexes are $Pt^{(IV)}$ complexes presenting amine derived ligands as non-leaving groups. Different requirements must be considered for the design of these drugs. Looking to an adequate value for light activation, or not to be reduced before it comes to target sites are key factors.

As in the case of cisplatin, chlorine has been used as axial ligand and iodine has been proposed as leaving group, unfortunately no objective treatment was achieved due to the presence of the active complex without any irradiation.[8] Due to the importance of the influence of the axial ligand, other options as acetate were tested, but the active form was still present. It was concluded that it was a product of biological reducing agents such as glutathione and N-acetylcysteine via inner sphere mechanism.[9] Introduction of azide ligands as leaving ligands cause a generation of photoactivated

Pt$^{(IV)}$ drugs, in which a change of axial or amine non leaving ligands leads to a different promising ligand.[10]

In this work, some of the most promising complexes will be theoretically evaluated achieving a response for the transitions responsible of drug activation and why they are activated beyond the maximum calculated transition. Spin-orbit contribution is taken account to explain experimental behavior of complexes, to obtain new transitions that are not present on UV-Vis spectrum due singlet-triplet transitions are not allowed on this spectroscopy. As well, possible docking of these drugs with DNA was simulated by using AutoDock 4 for a blind dock. Then for a more in-depth interaction, different parameters were set on ORCA quantum chemistry package.

I.2   Problem Statement

Even the continuing evolution of chemotherapy drugs, there still present some problems as the lack of a targeted drug to cancer treatment, drug side effects, and the resistance of pre-established treatment. It is imperative new approach at the design of anticancer drugs, as an understanding of the mechanism of action leading this study to focus on a better understanding of promising photoactivated platinum(IV) anticancer drugs, the influence of their ligands and their possible interaction with DNA establishing a possible action pathway.

One of the great challenges of this study is to get an accurate proposal for docking of the activated drug with DNA and propose pathways responsible for drug formation without putting away reported approaches for drug activity.

I.3   General and Specific Objectives

This thesis work states as a general objective the performance of a theoretical study of promising photoactive platinum-based drugs leading to a better understanding of their activity by considering spin-orbit contribution and possible docking results explaining its biological activity. To make it realizable specific objectives must be accomplished listed below:
- o   Geometry optimization by using Orca.
- o   TDDFT excited states calculation using previously calculated coordinates.
- o   Determine the influence on activation energy shift from complexes considering Spin-Orbit contribution.

- o By blind AutoDock, determine the active site preferred by the complex with DNA.
- o Determination of the strong interaction between specific nitrogenous base and platinum complex.

Chapter II Theoretical Framework

In this chapter are introduced the different theoretical concepts useful for this work.

II.1 Electronic transitions in inorganic complexes

II.1.1 Types of transitions

Electronic spectroscopy (UV-Vis spectroscopy) is a useful tool to characterize metal coordination complexes. Information obtained from this spectroscopy is richest compared to that for organic compounds due to the presence of d electrons. Among the electronic transitions that we can observe for the coordination compounds are the following:

Metal-centred (MC) d-d transitions are included here, which are governed by Laporte and Spin forbidden rule. It is well known that MC transitions typically populate antibonding orbitals, causing a bond lengthening giving rise ligand substitution.

Charge-transfer (CT) transitions as metal to ligand (MLCT), ligand to metal (LMCT), and to solvent (TS) are considered here. CT transitions lead redox reactions and in homolytic cleavage, which leads to the production of radicals and so on the reduction on the metal.

Ligand-centred (LC) transition. Only involve interligand transitions that could be seen in delocalized systems.[6]

II.1.2 General mechanisms of excitation

Using Jablonski Diagram (**Figure 1**), the excitation and decay pathways could be illustrated. The first step is the absorption of light irradiated, and usually a singlet state goes to an excited singlet stated, which state remains nanoseconds making it too short to cause a notable difference. For decay pathways, S_1 state is stabilized by the emission of radiation returning to a basal singlet state (S_0), which is known as fluorescence. Or by a non-radiative process via intersystem crossing, which comes from an excited singlet state (S_1) to a triplet state (T_1) with emission of heat, triplet (T_1) state then is stabilized with the emission of radiation returning to the basal singlet state, this phenomenon is known as phosphorescence. Phosphorescence lifetime is more extensive compared to fluorescence, which is sufficient to interact with surrounding species and initiate a photodynamic reaction. Such scheme allows us to know the process of excitation and decomposition of the drug. Even though there are two

different types of photoactivated drugs, the one is briefly described above an is related to photodynamic therapy (PDT), which is maintained after light irradiation and photoactivated chemotherapy (PACT) drugs that are which become active after light irradiation due they decompose. Although another difference is that PDT mechanism has as requirement oxygen presence, and PACT acts even when there is no presence of oxygen. [11] This has become very important due to on tumors sites, the presence of oxygen is low.
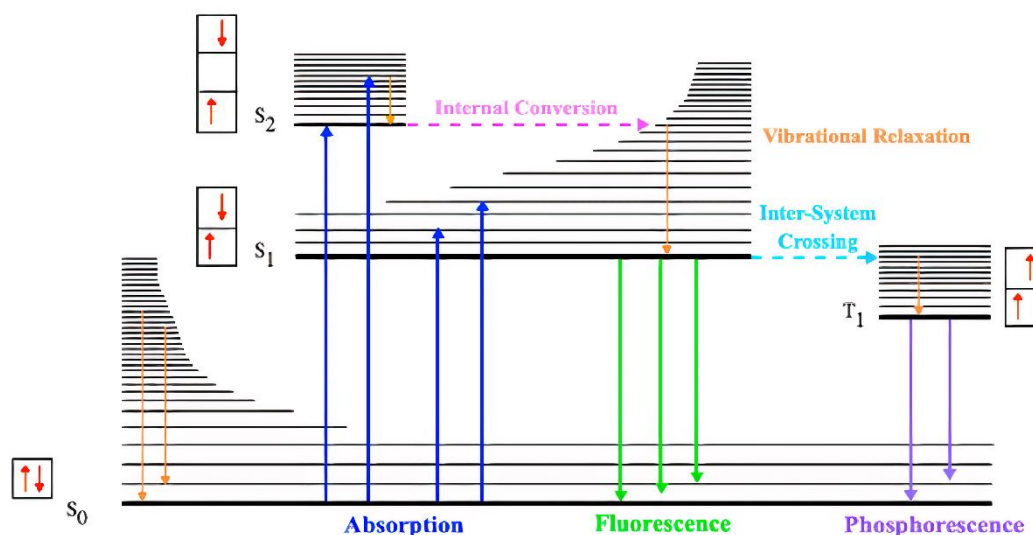
Figure 1: *Jablonski Diagram*

The reaction mechanism of cisplatin before binding to DNA is well known, the first step is that the complex pass through an aquation process named the activation process. $Pt^{(IV)}$ photoactivated octahedral complexes owns another process of activation, in which perfunctorily reduces to $Pt^{(II)}$ and losses its axial ligand, to then be hydrolyzed and interact with DNA.[12] Platinum photoactivated drugs undergo different mechanism of decomposition of $Pt^{(IV)}$ complexes as photo-substitution, photoreduction, photo-switching or photoisomerization depending on their ligands.

II.2 Mechanism of biological activity of inorganic complexes
II.2.1 Appropriate UV length value

When light is applied to the skin, not all the light is absorbed also it is reflected, transmitted, or scattered. The presence of elements with different characteristics as density, scatter the light before it reaches the drugs. Also, the light could be absorbed by other absorbing dye, such as hemoglobin or melanin. Even though that all tissues are not the same, in most tissues with lower energy ranges is reached a deeper penetration of light. Phototherapeutic window is in the range from 620-850 nm, in

which is reached the maximum penetration rate at mammal tissue.[13] There is another factor that influences the penetration of the light, when the beam width comes broader also increases the penetration deep. It must be taken into consideration that there will be a point in which the increase of width would not affect penetration rate.[14]

II.2.2 ADN Cleavage

There are general processes of how anticancer complex cleavage to DNA, as interstrand, intrastrand, and monoadduct. Interstrand crosslink is a DNA lesion that involves a covalent interaction with both strands of DNA. This lesion impedes the DNA strands to separate and undergo the replication process, also prevents the access of repair enzymes and transcription factors. Cisplatin, carboplatin and oxaliplatin cause this lesion at DNA.[15] Cisplatin interact covalently with the N7 site of deoxyguanosine residues of both DNA strings.[16] It is well known that the most common DNA targets are N7 site of guanine and exocyclic N2 site of guanine, that represent the nucleophilic attack to electrophilic alkylating agents.[17,18]

Interstrand crosslinks also prevent DNA separation when an agent connects covalently with two nucleotide residues of the same DNA string.[17] Monoadduct damage refers to when an agent only binds to a single base.[18] DNA adducts localization depend on the characteristics of the adduct, as the size, or the electrophilicity of the agent. If the agent is a strong electrophile, it displays a greater ranger on nucleophilic targets.[19]

II.3 Photoactivated Platinum (IV) Complexes as promising anticancer drugs
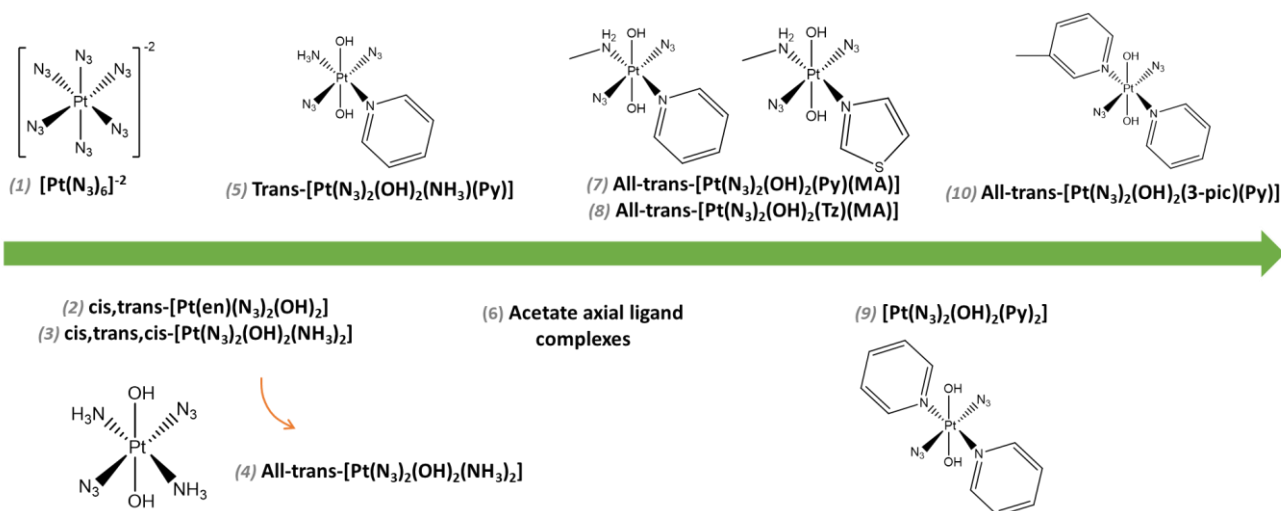
Figure 2 Photoactivated Platinum(IV) prodrugs with time

Platinum base drugs represent 50-70% of chemotherapy treatment since the discovery of cisplatin[20]. Due to the resistance that cells develop against these complexes, the continuous development of new drugs is essential. Also, another obstacle to overcome is cancer target's deficiency of approved drugs. To overcome this, photoactivated $Pt^{(IV)}$ complexes have raised interest owing to its lower cytotoxicity and being stable under physiological conditions without light exposure. [21] Moreover, it has been proved that octahedral, low spin d^6 $Pt^{(IV)}$ complexes are inert to substitution with biomolecules out of interest. Iodide-based $Pt^{(IV)}$ prodrugs were first reported in the 1990s, it has presented high cytotoxicity upon light radiation but also presents comparable cytotoxicity without light irradiation. Its cytotoxicity in the dark also is attributed to biological reducing agents as glutathione (GHS) or ascorbic acid. [12] Its instability on the dark is due iodine is a weak field ligand making the LMCT bands on a relatively longer wavelength,[8] making easier (less energetic) to donate electrons there. On the development of Iodide-based $Pt^{(IV)}$ prodrugs, the influence of axial ligands on complexes reduction potential was shown as well as their stability.[22]

To overcome this problem, diazido-based $Pt^{(IV)}$ complexes have raised interest due to the absence of significant cytotoxicity in the dark, as also their activity upon light irradiation. [11] The first complex with an azido ligand was diazidotetracyanoplatinate[(IV)] reported in 1978 by Vogler *et al*., which at light exposure ($\lambda \approx 300nm$) undergo to a trans reductive elimination of N_3 radicals without the formation of $Pt^{(III)}$ intermediate.[23] After the formation of azidyl radical, it decomposes on nitrogen gas, making it more difficult to re-oxidation of the metal center. [24] Since it, more remarkable generation of complexes are presented on *Figure 2*, labeling each complex that will be described with a number.

In 1983, $[Pt(N_3)_6]^{-2}$ **(1)** was synthesized, which presented a LMCT band ($N_3 \rightarrow Pt$) at 308 nm. Irradiation on the LMCT band gives $[Pt(N_3)_4]^{-2}$ product, and if the irradiation is continued, the precipitation of colloidal Pt was seen with the presence of bubbles that were attributed to nitrogenous gas. [25] In this way, it was demonstrated that only two azido ligands must be present to become active if all the azide ligands are released due to its lability making the complex inactive. The following azido complexes reported have the formula $[Pt(N3)2(L)(L')(OR)(OR')]$, in which different axial ligands as acetate or hydroxyl were coordinated. [11] On 2003, two azido-complexes were synthesized, *cis,trans*-$[Pt(en)(N_3)_2(OH)_2]$**(2)** and *cis,trans,cis*-$[Pt(N_3)_2(OH)_2(NH_3)_2]$ **(3)**.[26] These two complexes were used to treat human urinary bladder cancer cells for 6 hours in the dark, and no significant inhibition of growth was seen. After complexes irradiation at 366 nm for 6 hours, inhibition of cell growth was

seen. Both complexes showed less toxicity than cisplatin, which was expected, but it was remarkable that both azido complexes are equally toxic to 5637 and cisplatin-resistant 5637 cells, which means a different mechanism of action.[10] Knowing that both complexes only change on their amine ligands, it was determined that the axial ligand (OH) was responsible for the stability having a big impact on the reduction potential, as well the influence of the amine ligands determine the lipophilicity and the DNA adducts of the drug. [27]

A change in the geometry from *cis,trans,cis* to all-*trans*-$[Pt(N_3)_2(OH)_2(NH_3)_2]$ **(4)** had represented an enhancement on the cytotoxicity reaching the potential of cisplatin, irradiating trans-complex for a short time. In the absorption spectrum, a bathocromically shift of LMCT band was seen from the *cis*-to the *trans*-complex, going from 256nm to 285nm; also, an increment of signal intensity is shown[28]. Basing on this, higher activity of *trans* complex could be attributed, which requires less energy and ensure deep penetration of radiation, making reduction more feasible. This fact contrasted the classical fact that *cis* geometry was more favorable since it diazido-based Pt complexes with different amine ligands had demonstrated to be more potent on its *trans* configuration.[11] There is also present reactions of photosubstitution and photoisomerization before photoreduction of *trans*-$[Pt(N_3)_2(OH)_2(NH_3)_2]$, that when it is coordinated the only product obtained was *trans*-$[Pt(NH_3)_2(N7-5'-GMP)_2]$, while complex with *cis*- configuration gives *cis*- and *trans*- products.[28]

Then in order to reach a better understanding of the *trans* complex, one of the *trans* amine ligand was replaced by pyridine as a bulky steric ligand that hind the metal center from reducing agents. *Trans*-$[Pt(N_3)_2(OH)_2(NH_3)(Py)]$ **(5)** showed a little bathochromic shift concerning *trans*-$[Pt(N_3)_2(OH)_2(NH_3)_2]$[12], as well a significant increase on cytotoxicity maintaining its inactivity on the dark. A minimum irradiation time was obtained; 30 minutes under UVA irradiation (λ=351nm) were found optimal to activate the drug. The process was monitored with ^{14}N NMR spectroscopy, showing that after 30 minutes of irradiation, azides have been released, as well no presence of free pyridine was detected, suggesting that it plays a recognition role on DNA adduct. Even though, on some adducts no recognition was attributed to pyridine, as in the case of DNA-GN7 adduct for *cis*-$[Pt(NH_3)_2(Py)]^{2+}$ that after photoisomerization and the formation of mono-adduct the presence of pyridine was the responsible for blocking the RNA polymerase. Computational calculations have shown LMCT transition bands on UV region and have determined the presence of some weak LMCT transitions on UVA and visible region. Complex **5** presents a dissociative nature due they are contributions for σ-antibonding LUMO and LUMO+2 orbitals, where LUMO presents the major antibonding character

for Pt-N_3 bonds. This explains the activation by visible light and the azide release. [29] Due to all its qualities, it is the only complex that has been proved in vivo on mice nude mice bearing xenografted OE19 tumors, showing antitumor activity upon irradiation.[11,22] In addition, the replacement of pyridine ligand with another amine ligands as piperidine did not show significant differences in its activity.[30]

As complexes **4** and **5** have similar LMCT transitions bands, both of them after long periods of UVA irradiation suffer the loss of their amine ligands, increasing the pH of the medium and reducing the activity of the drug, as well the loss of their spectator ligands reduce its activity due to the influence of this ligands on the solubility of the complex. [12] To avoid this drawbacks, there different complexes with different amine ligands were synthesized *trans,cis*-[Pt(bpy)(OAc)$_2$(N$_3$)$_2$](bpy=bipyridine); *trans,cis*-[Pt(phen)(OAc)$_2$(N$_3$)$_2$](phen=phenanthroline); and *trans, trans, trans*-[Pt(OAc)$_2$(N$_3$)$_2$(py)$_2$], in which the axial ligand was acetate **(6)**. It was demonstrated that the acetate free Pt$^{(II)}$ complexes were achieved after UVA irradiation(365nm) and upon exposure of green light (514nm). It was accordingly becoming reactive aqua species after azide release. After irradiation, not change of pH was detected as [Pt(N$_3$)$_2$(OH)$_2$(NH$_3$)$_2$] and [Pt(N$_3$)$_2$(OH)$_2$(NH$_3$)(Py)] produced after light exposure.[31] Owing to the fact that it absorbs on the visible region, it makes these complexes better candidates for photoactivated chemotherapy. As well that not pH increase is detected, it could be related to changing the conformation of amine ligands.

Higher potent complexes were introduced, having methylamine ligands (MA). Zhao *et al.* introduced *trans,trans,trans*-[Pt(N$_3$)$_2$(OH)$_2$(Py)(MA)] **(7)** and *trans,trans,trans*-[Pt(N$_3$)$_2$(OH)$_2$(Tz)(MA)] **(8)**, where Tz is a thiazole ligand. Both complexes presented great stability under dark, and they did not react with ascorbic acid or 5'-GMP on aqueous solution for three days. Even though they have reacted slowly with glutathione, only a 2% to 10% reacted after this time. Experimental UV-VIS of both complexes showed maximum absorption at 289nm, which correspond to N$_3$→ Pt$^{(IV)}$ CT band, and other transitions going to the visible region. Irradiation of complexes using 365,420 and 450nm has decreased the 289nm band indicating the loss of N$_3$-Pt bond. TDDFT calculations were carried out showing a better understanding of transitions, weak transitions were found at 420-430 nm region that presented an σ-antibonding LUMO's contribution explaining dissociative character of the excited state. In the UV region, most transitions seen were attributed to LMCT bands. Triplet states were found to be azide releasable, indicating an intersystem crossing process. Phototoxicity of these complexes was evaluated in different cell lines as keratinocytes (HaCaT), cisplatin-sensitive (A2780) ovarian carcinoma cells, the cisplatin-resistant (A2780CIS) and OE19 oesophageal adenocarcinoma. After irradiation of complexes using UVA light (λ=365nm), cytotoxicities have increasingly becoming more

potent than cisplatin achieving a high toxic result on the cisplatin-resistant A2780CIS cell line. Additionally, blue light was found optimal to the activation of both complexes producing other cytotoxic biological chromophores as porphyrins. Thiazole containing complexes have demonstrated a crucial factor decreasing resistance factor for cisplatin-resistant cell lines (A2780/A2780CIS) compared to complexes containing only pyridine ligands. Besides including methylamine group instead of amine ligand was demonstrated increased UVA phototoxicity.

Different structures have been found after irradiation in the presence of 5'GMP. ^{1}H NMR spectroscopy and HPLC were used to identify different photo-products, for *trans,trans,trans*-$[Pt(N_3)_2(OH)_2(Py)(MA)]$ complex, the major product formed after 1 hour of irradiation was (SP-4-2)-$[Pt(N_3)(MA)(Py)(5'GMP)]$ and the minor product was *trans*-$[Pt(MA)(Py)(5'GMP)_2$-2H]. For *trans,trans,trans*-$[Pt(N_3)_2(OH)_2(Tz)(MA)]$ after 15 minutes of irradiation, the major product formed was (SP4-3)$[Pt(N_3)(Tz)(MA)(5'GMP-H)]$, and the minor product was *trans*-$[Pt(MA)(Tz)(5'GMP)_2$-2H]. After the times mentioned above, where it has been seen that the complexes have reacted almost wholly, the MA release is minimum. Based on these results, it has been indicated azido released as azidyl radical besides hydroxide release being electron donors responsible for $Pt^{(IV)}$ reduction to $Pt^{(II)}$. Less frequently it was also found that the complexes lost both azide ligand forming bis-5'GMP adduct, these type of adducts were more present when irradiation time with UVA light was continued after complete reaction.[32]

It was also introduced a new complex having as ammine ligands pyridine, $[Pt(N_3)_2(OH)_2(Py)_2]$ **(9)**, in which referring to the previously mentioned complex, it has changed acetate ligands to hydroxyl ligands. Selecting the OH as axial ligand makes the complex more difficult to de reduced by biological agents, its influence can be attributed to the size and electronegative of OH generating a bigger splitting in the octahedral field making more challenging to place electrons on e_g orbitals[12]. $[Pt(N_3)_2(OH)_2(Py)_2]$ has shown greater thermal stability compared to $[Pt(N_3)_2(OH)_2(NH_3)(Py)]$, that decomposes at a temperature above 453 K. As well, it has presented good stability in the presence of GSH in the dark being 70% of the complex unreacted after one week. Irradiating bipyridine complex using 365 nm radiation has shown phototoxicity on different human cell lines as keratinocytes (HaCaT), parental(A2780), and cisplatin-resistant(A2780CIS) ovarian carcinoma, among others. In the HaCat cell line, 420 nm radiation was used presenting an order of magnitude more than cisplatin. The dependence of an appropriate wavelength for activation of $Pt^{(II)}$ complexes has three major factors as its accumulation, its quantum yield, and the toxicity of all photo products at every wavelength.[33] When

it is referred to the quantum yield, it measures the number of events over the number of photons absorbed, in this case, the number of events becomes the number of $Pt^{(II)}$ active complexes formed after irradiation.[34]

Differently from complexes that have lost its ammine ligands after irradiation three wavelengths (350nm, 420nm, and 450nm) were employed, demonstrating no pyridine release after irradiation. Due to this, it is probable that the presence of NH_3 ligand causes the amine release in previous complexes. TDDFT calculations were obtained for a better understanding of transitions responsible for complex activation. On the UV spectrum region were present important contributions, as a dissociative LMCT($N_3 \rightarrow Pt$) band and a mixed LMCT/IL(IL=interligand) transition. Also, transitions on the visible region were found to have dissociative character and be of LMCT/IL mixed character. Furthermore, ground triplet state geometry shows the dissociative character of azido ligands[33], implying an intersystem crossing pathway. [35]

With the intention of determinate DNA photo-adduct formed after irradiation, 5´-GMP is used in the presence of the compound knowing that the favorite target of DNA is guanine. Using irradiation of 420nm leads to a quick decrease of concentration of octahedral complex that after being elucidated with Pt NMR, it has shown the formation of three different complexes. It is believed that in order of the major to the minor product formation is: *trans*-$[Pt(N_3)(py)_2(5'\text{-}GMP)]^+$, *trans*-$[Pt(py)_2(5'\text{-}GMP)_2]^{2+}$ and $[Pt(N_3/OH)(OH)_2(5'\text{-}GMP)(py)_2]^+$. Only the middle product was confirmed, and the two remaining were established with the analogy of photoactivity of *trans,trans,trans*-$[Pt(N_3)_2(OH)_2(NH_3)(py)]$.[33]

Based on the bipyridine complex, a series of heterocyclicimine $Pt^{(IV)}$ complexes have been synthesized and characterized. Heterocyclicimine ligands used were thiazole, 1-methylimidazole, and different methyl picoline ligands. Each one showed different results, introducing a promising complex that has as ligands a pyridine and a 3-picoline. *Trans,trans,trans*-$[Pt(N_3)_2(OH)_2(3\text{-picoline})(pyridine)]$ **(10)** complex present two absorption bands, a more intense band is seen experimentally at approx. 295nm. and a less intense band at approx. 265nm. Photoactivity of the complex was evaluated under blue and green light, under blue irradiation light at 463nm, the most intense band corresponding to LMCT $N_3 \rightarrow Pt$ has decreased over time. Furthermore, it was evaluated under green light irradiation at 517nm, and it has shown a slow decrease of most intense band implying the loss of N_3 ligand.[36]

Under the presence of 5′-GMP and irradiation of light(420nm), the presence of Pt adducts were determined by ^{1}H NMR spectroscopy. After irradiation, no presence of heterocyclic ligands was determined. The percentage of formation of 5′-GMP binding adducts with complex was determined by ^{1}H NMR (58%). Picoline derived complex does not present cytotoxicity without light irradiation; however, it presents greater phototoxicity against cisplatin-resistant(A2780CIS) ovarian carcinoma than the previously mentioned bipyridine complex. Complex (3-pic,py) showed remarkable phototoxicity against the OE19 cell line compared with heterocyclicimine ligand-based complexes.[36] Taking account the potent phototoxicity against this cell line and considered that oesophageal cancer is superficial, the use of photochemotherapy using UV shifted wavelengths is an up-and-coming option.

II.4   Spin-Orbit Coupling as an explanation for the origin of photo reactivity

Aiming an explanation of doublet signals present on emission spectrums of different atoms that only haves one valence electron, spin-orbit coupling was the reason. Spin-orbit coupling is a relativistic interaction, where based on the Bohr atomic model, the center is occupied by the electron instead of the nucleus. Nucleus(Z_e), positively charged is orbiting around electron creating a positive current loop that turns into a magnetic field (**B**), which direction is given by the right-hand rule (*Figure 3*). Electrons present an intrinsic property, electron spin that creates spin angular momentum and induces a spin magnetic dipole moment (μ_s). When electron spin magnetic moment is placed into the magnetic field (**B**), it creates a torque force driving magnetic dipole moment to B field alignment. As a result of this interaction, there is the degeneracy of energy levels electrons, in which energy is represented on the following equation.

$$H_{SO} = \Delta E = -\mu_s \cdot \mathbf{B}$$

The magnetic moment is proportional to the spin angular momentum (*s*); therefore, we have:

$$\mu_s = -\frac{e}{m_e}\mathbf{s}$$

And the magnetic field (B) is proportional to the orbital angular momentum (l),

$$\mathbf{B} = -\frac{\mu_0 Z_e}{4\pi m_e r^3}l$$

In this way, spin-orbit coupling could be defined as the interaction of the spin angular momentum and the orbital angular momentum. Winding up that energy degeneracy is proportional to this interaction.
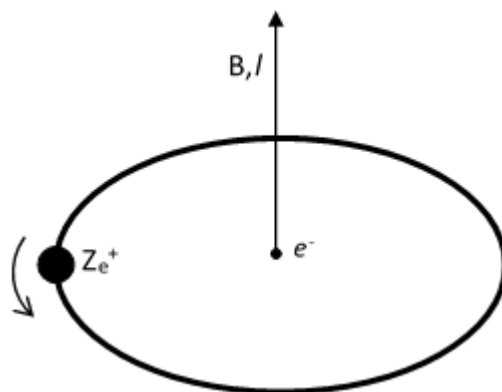
Figure 3 Spin-Orbit Coupling

II.5   Computational methods as an exploratory tool

On latest version of ORCA quantum chemistry program, it is possible to include Spin-orbit coupling between excited states to which computation could be done including solvent. [37] Spin orbit coupling has been used to calculate radiative rates for nine ruthenium complexes with good approximation to experimental reported values. Methodology employed was spin-orbit coupled to time-depend density functional theory (TDDFT), including relativistic approximation ZORA. Using singlet ground state geometry and TZVP level of theory, a more accurate result is obtained. [38]

Chapter III Methodology

Computational details for each step are described below.

III.1   General considerations of calculations

The availability of different programs that are used as tools on computational chemistry makes it a more suitable accessible research area. An example is Avogadro, which is a visualizer tool and molecule editor that can be used on different platforms for molecular modeling, bioinformatics, among other research areas.[39] Avogadro has the capacity to reproduce extensible input files that can be used for optimization of geometries using quantum chemistry software as Orca, in which different methods and basis sets can be set.

Orca is a quantum chemistry program package that presents modern electronic structure methods ranging from density functional theory (DFT), many-body perturbation, semi-empirical methods, etc.

The principal field of application are transition metals, larger molecules, and their spectroscopic features.[37] Basis set, methods and correlation factors used for the theoretical study are listed below:

PBE0 is a hybrid functional in DFT that incorporates a portion of exchange Hartree-Fock theory with an exchange-correlation interaction model. PBE0 functional is an integer by Perdew–Burke-Ernzerhof (PBE) and Hartree–Fock exchange energy in a proportion of 3:1, with full PBE0 correlation energy. [40]

def2-TZVP (Valence triple-zeta polarization) basis set is highly recommended for light elements even when a heavier element is present. By this basis, energies and geometries are fairly converged at DFT level. [41]

ZORA (Zeroth-order regular approximation) is a scalar relativistic method in DFT that takes into consideration all electro calculations. ZORA aims a set of segmented-all-electron- relativistic contracted (SARC) basis set for third-row transition metals. [37]

DOSOC Spin-orbit coupling between singlet and triplets can be calculated from DFT by using a quasi-degenerate perturbation theory. SOC calculated states are between excited singlet states and spin-adapted triplets.[42]

D3BJ is a dispersion correction in DFT calculations, is important at the moment of treating noncovalent interaction which is dominated by potential energy surfaces.[43]

AutoDock is a free software for an automated dock for small ligand with a receptor protein. AutoDock 4 consists of two main programs, AutoDock performing ligand searching minimums at grids describing the protein and AutoGrid that creates mentioned grids. [44]

III.2   Geometry Optimization

Using Avogadro as a visualization tool, complexes of interest were designed. Using extensible Avogadro´s tool to generate input files, the method used for all complexes was PBE0. PBE0 is highly recommended for transition metals below the first-row transition metals giving more reliable energy or properties of metal complexes. PBE0 is the best candidate due it has the necessary contribution of Hartree–Fock exchange and it will affect directly to the bond that is formed by the metal.

Def2-TZVP was chosen as basis set due it makes calculation more reproducible, and studies indicate that using PBE0 with a triple-zeta basis set gives reliable results for geometries. All previously mentioned methods are presented on *Figure 4*.

```
# avogadro generated ORCA input file
# Basic Mode

! PBE0 OPT def2-TZVP

* xyz 0 1
  Pt     -0.27668      0.41035     -0.17843
  N      -2.27402     -1.77452     -0.11998
  N      -3.14092     -2.19126      0.45385
  N      -1.23675     -1.27490     -0.80875
  N       0.66255      2.11187      0.46598
  N       1.85005      2.50419     -0.01944
  N       2.84275      2.83352     -0.42029
  N       1.25993     -0.59491      0.78104
```

Figure 4 Input for Geometry optimization.

III.3   TDDFT calculation (Excited states)

A new input for TDDFT excited states was generated using coordinates obtained from the output of ORCA after the geometry optimization was achieved. The same functional and basis set were used, now adding RIJCOSX approximation, which takes into consideration Coulomb integrals and COSX numerical integration for HF exchange, that renders calculations more feasible without affecting the accuracy of calculations conducted with hybrid functional. Excited states were performed in water as solvent, adding to the input CPCM(water). Previously mentioned parameter to the input are seen on *Figure 5*.

```
# avogadro generated ORCA input file
# Basic Mode

! PBE0 def2-TZVP def2/J RIJCOSX Grid5 FinalGrid6 TightSCF CPCM(water)
%maxcore 1000
%tddft
  maxdim 5
  nroots 50
end
%output
Print[ P_Basis ] 2
Print[ P_MOs ] 1
end

* xyz 0 1
  Pt     -0.27668      0.41035     -0.17843
  N      -2.27402     -1.77452     -0.11998
```

Figure 5 Input for TDDFT calculation.

III.4   Evaluation of Spin Orbit Coupling contribution

For SOC contribution, the same input for TDDFT calculation was used with some modifications. ZORA scalar relativistic is a method that is recommended to heavy elements and can be used without any inconvenient with TZVP basis set, it is widely recommended so it is applied only for platinum atom.[42] As well auxiliary basis set SARC/J is used. SOC contribution is calculated by adding DOSOC TRUE. Previously mentioned statements are employed (*Figure 6*) due they present good accuracy to SOC contribution for Ir complexes.[38]

```
# avogadro generated ORCA input file
# Basic Mode

! PBE0 ZORA ZORA-def2-TZVP RIJCOSX SARC/J Grid5 FinalGrid6 TightSCF CPCM(water)
%maxcore 1000
%tddft
   maxdim 5
   nroots 50
   DOSOC   TRUE
end
%basis
NewGTO Pt "SARC-ZORA-TZVP" end
end
%output
Print[ P_Basis ] 2
Print[ P_MOs ] 1
end

* xyz 0 1
  Pt     -0.27668      0.41035     -0.17843
   N     -2.27402     -1.77452     -0.11998
```

Figure 6 Input for Spin-Orbit contribution.

III.5 Protein docking using AutoDock

As DNA sequence, 1BNA was used with few modifications in order to obtain two adjacent guanine nucleotides, two adenine nucleotides, and Adenine-Guanine adjacent nucleotides. As the first step, Auto grid must be run before AutoDock; at this point, pre-grid maps are generated for the DNA, which is the receptor. In order to generate pre-grid maps, non-polar hydrogens must be removed, and Gastering charges were added to DNA. For the ligands, platinum complexes, Hirshfeld partial charges were calculated in Orca.

In this particular case, in the parameter file for AutoDock 4, there is not a platinum atom. A parameter file containing platinum atom was set. Grid box dimension was defined, where the area of interest of DNA was put inside. Now AutoDock is run, number of dockings established was 70 iterations, and the output file was in the Lamarckian genetic algorithm (LGA), which handles a large number of degrees of freedom for flexible docking. In this case, blind docking is performed, so the first grid box was established including a large number of nitrogenous bases, then a square point is located, and the process is repeated in a small pointed grid box.

A more realistic result is achieved when the most interactive part of DNA is cut and included with the complex in an aqueous medium, and energy optimization is performed to obtain more possible interactions. The same functional and basis set used for geometry optimizations were established, but the D3BJ dispersion factor is added) (***Figure 7***).

```
# avogadro generated ORCA input file
# Basic Mode
#
! PBE0 OPT D3BJ def2-SVP CPCM(water)

* xyz 1 1
    P       16.55093      -8.89939       1.53730
    O       17.30407     -10.08785       0.87944
    O       17.74631      -8.53770       2.45953
    O       17.01330      -7.74874       0.31145
    C       16.22579      -7.94164      -0.83578
    C       16.92415      -7.39664      -2.09415
    O       17.03489      -5.99120      -2.01455
    C       18.32948      -7.98049      -2.31932
    O       18.55995      -7.98888      -3.70884
```

Figure 7 Input for QM region calculation.

III.6   General procedure for the complete theoretical study

All complexes conformations were first optimized, then with their optimized coordinates from output it was generated another input to obtain TDDFT results, and also same procedure was applied for SOC contribution, as previously mentioned. With this results UV-Vis spectrums were obtained. Then, same procedure of optimization was developed for complexes without one azide. And TDDFT also were carried out to know strong dissociate contacts in order to a better elucidation of docking complex under light exposure. AutoDock process were carried out and finally, the more interacting zone obtained from AutoDock was inputted into ORCA to a better understanding of more probable interactions. A general scheme of all procedure is seen on *Figure 8*.
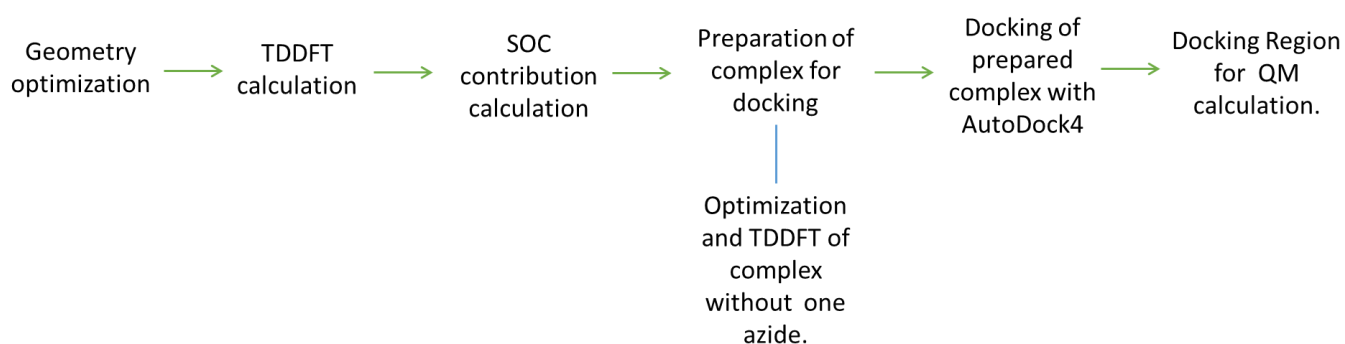
Figure 8 General scheme for complete theoretical study.

Chapter IV : Results and Discussion

The aim of this part is to present the different steps necessary to calculate and propose a potentially anti-cancer drug. The starting point is the selection of potential active complexes, then evaluate their photo-reactivity and finally find where these complexes would be present through protein docking.

IV.1 Primary phase of selection of potentially active complexes

As explained before, cisplatin is a well-known anti-cancer drug and a wide range of Pt-containing complexes were recently synthesized. Pt atom seems to be an indispensable ingredient of these anti-cancer drugs, and new prodrugs with platinum[IV] has raised great research interest. Another indispensable factor is the amine based ligands that influence in the solubility and photoactivity of each complex. In addition, amine derived ligands could be closely related to its interaction with DNA ergo its cytotoxicity. Bearing in mind that for a promising complex, optimal light for drug activation must be on the visible range and must present considerable cytotoxicity against resistant cisplatin cell line, due this four complexes were selected for the theoretical study. Four complexes are complex **7**, **8**, **9**, and **10** presented on *Figure 9*.
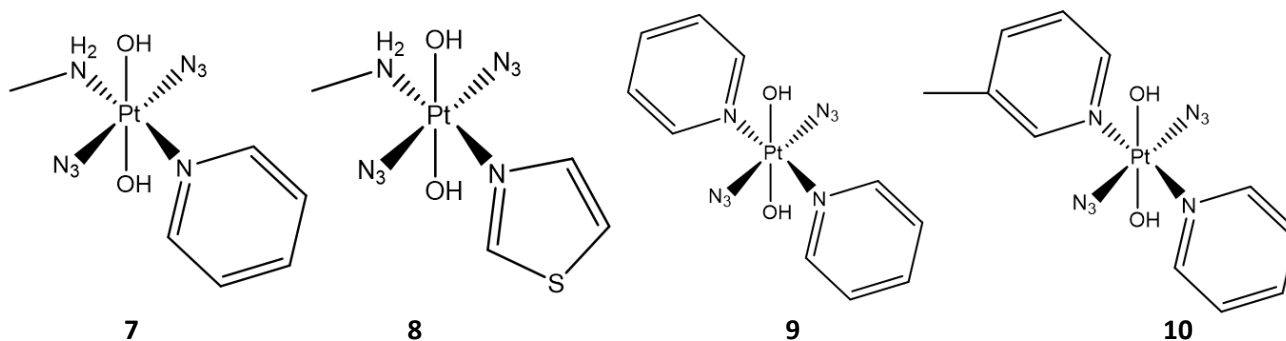
Figure 9 Computational studied complexes.

IV.2 Structural and electronic features of selected potentially active complexes

IV.2.1 Optimized structures

Geometry optimization structures were obtained for singlet and triplet ground states, with great concordance with reported bond distances.[11,33,36]

Complex 7: *Trans,trans,trans*-[Pt(N₃)₂(OH)₂(Py)(MA)]

For complex **7**, *Table* 1 and *Table 2* present figures of both conformations and bond distances (Å) formed by platinum of each conformation, respectively. A difference of 3,22KJ/mol between the two conformations were obtained, making impossible to determine which is the most favored. Main differences between the two conformations were azide and methyl (MA) orientation. Also the distances between azides and platinum, or hydroxyl and platinum do not present big differences. The two conformations present a notable elongation of azide ligands on its more stable triplet geometry.

Singlet ground State	
Conformation 1	Conformation 2
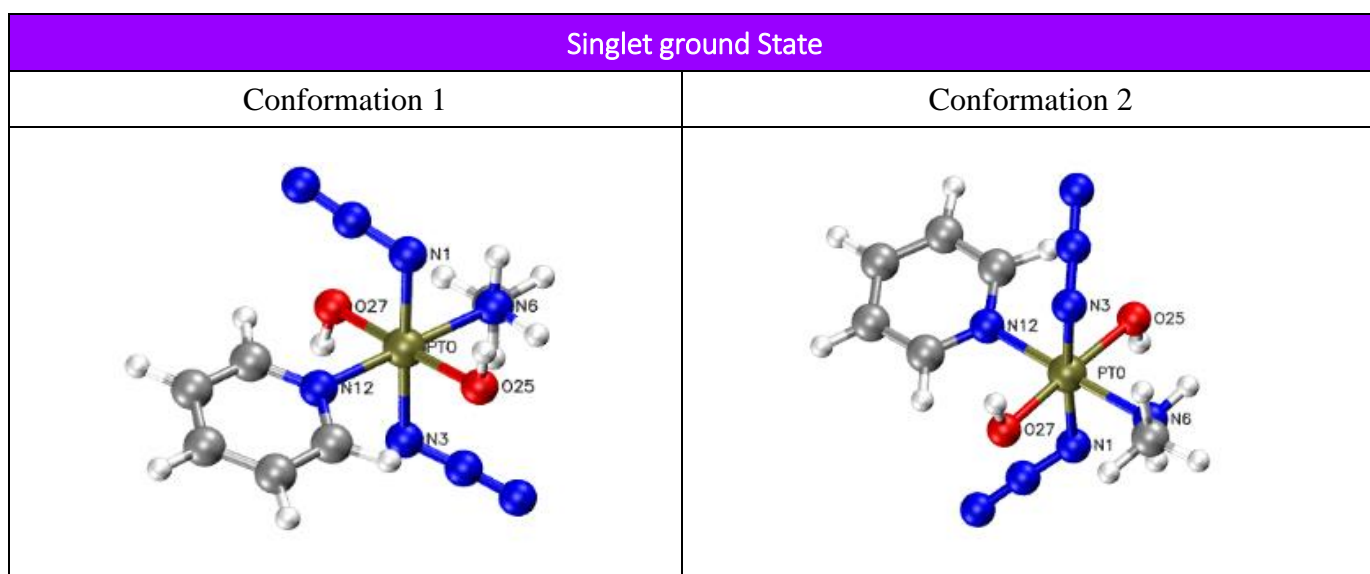
Table 1 <u>Complex 7</u> - *Trans,trans,trans*-[Pt(N$_3$)$_2$(OH)$_2$(Py)(MA)] complex conformations.

	Singlet ground State	Triplet ground State
Conformation 1		
Pt-N3	2.0494	2.3706
PT-N6	2.0424	2.0630
PT-N12	2.0324	2.0438
PT-N1	2.0531	2.3611
PT-O25	2.0022	1.9935
PT-O27	1.9996	1.9616
	Singlet ground State	Triplet ground State
Conformation 2		
Pt-N3	2.0514	2.4389
PT-N6	2.0389	2.0542
PT-N12	2.0397	2.0418
PT-N1	2.0529	2.3799
PT-O25	2.0030	1.9972
PT-O27	2.0003	1.9660

Table 2 <u>Complex 7</u> - *Trans,trans,trans*-[Pt(N$_3$)$_2$(OH)$_2$(Py)(MA)] complex bond distances of each conformation.

Complex 8: [Pt(N₃)₂(OH)₂(Tz)(MA)]

Complex 8: [Pt(N$_3$)$_2$(OH)$_2$(Tz)(MA)]

An increment on bond distances between N$_3$-Pt is seen on triplet state of second conformation structure that has a concordance with favored azide release after light exposure. Between two conformations in their singlet geometry, in which the big difference is azide orientation, small difference is seen on bond distances. Instead, an increment of elongation of azide ligands on second conformation shows a strong release character of azide ligand on its triplet geometry. For complex **8,** bond distances are presented on *Table 4* and conformations are presented on *Table 3.*

Singlet ground State	
Conformation 1	Conformation 2
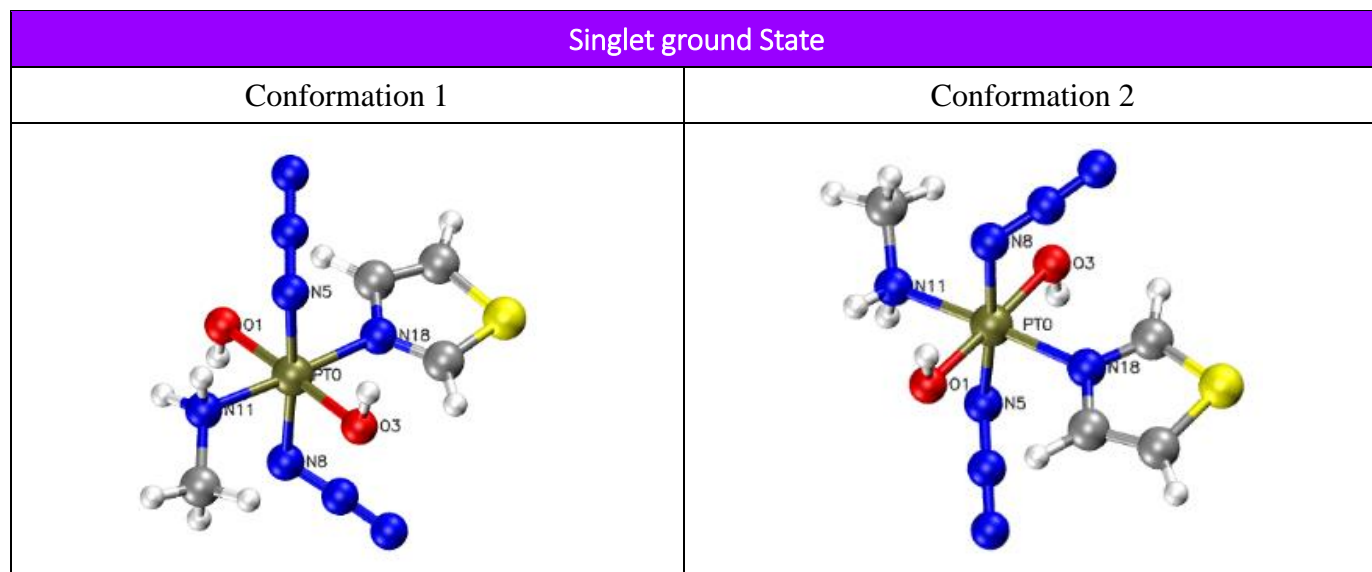
Table 3: Complex 8 - Trans,trans,trans - [Pt(N$_3$)$_2$(OH)$_2$(Tz)(MA)] complex conformations.

	Singlet ground State	Triplet ground State
Conformation 1		
Pt-N5	2.0514	2.0636
PT-N11	2.0345	2.3731
PT-N8	2.0530	2.0648
PT-N18	2.0249	2.4469
PT-O1	2.0011	1.9157
PT-O3	2.0033	1.9177
	Singlet ground State	Triplet ground State
Conformation 2		
Pt-N5	2.0517	2.2593
PT-N11	2.0348	2.0444
PT-N8	2.0527	4.4491
PT-N18	2.0251	2.0259
PT-O1	2.0009	2.0079
PT-O3	2.0033	2.0032

Table 4: Complex 8 - Trans,trans,trans - [Pt(N$_3$)$_2$(OH)$_2$(Tz)(MA)] complex bond distances of each conformation

On first conformation of complex **8** instead of elongation between azide-platinum bond, an increment on amine derived ligands is seen but not experimental amine ligand release has been detected. Based on the second conformation of complex **8**, it presents an energy difference with to previous mentioned conformation of 12.5324 KJ/mol which makes first conformation the most probable. However, energy difference is still low to determine a most favorable conformation, knowing that first configuration implies amine derived ligands that it is not seen experimentally.

Considering single point energy of more stable triplets' states between two conformations, the triplet state achieved by the second conformation is slightly more stable with a difference of 5.498 KJ/mol, which also is to low but it could be related that at this conformation the azide is already released, slightly explaining the more potent character than complex with pyridine instead of thiazole becoming rapidly active.

Complex 9: [Pt(N$_3$)$_2$(OH)$_2$(Py)$_2$]

For complex 9 two conformations were optimized. An aleatory geometry that gives first conformation after optimization. For the second configuration, two different input configurations were employed having the same final geometry optimization with a difference below 1KJ/mol so only one of these output is presented as second configuration. Conformations structures are presented on *Table 5*.

Singlet ground State	
Conformation 1	Conformation 2

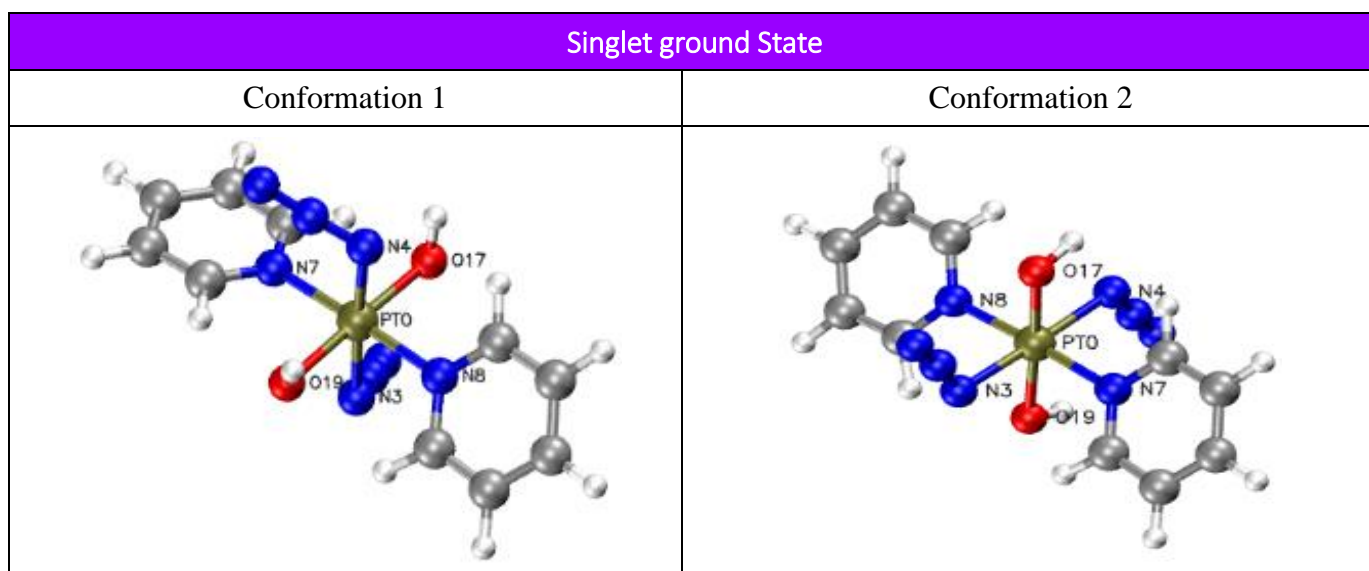*Table 5: Complex 9 - [Pt(N$_3$)$_2$(OH)$_2$(Py)$_2$] complex conformations.*

	Singlet ground State	Triplet ground State
Conformation 1		
Pt-N7	2.0456	2.0412
PT-N3	2.0462	2.4239
PT-N8	2.0205	2.0506
PT-N4	2.0615	2.3622
PT-O17	2.0007	2.0045
PT-O19	2.0078	1.9845
	Singlet ground State	Triplet ground State
Conformation 2		
Pt-N7	2.0244	2.3900
PT-N3	2.0476	2.0582
PT-N8	2.0247	2.3905
PT-N4	2.0641	2.0802
PT-O17	1.9958	1.9118
PT-O19	2.0080	1.9230

Table 6: Complex 9 - [Pt(N$_3$)$_2$(OH)$_2$(Py)$_2$] complex bond distances of each conformation

For complex **9**, *Table 6* shows bond distances formed by platinum on singlet ground states and in the more favored triplet state. On first conformation, bond distances increment on azide platinum leading to an understanding that a triplet state is reached favoring azide release. Moreover, on the second conformation bond distances is elongated between pyridine and platinum, which could lead to pyridine release that is not a feature seen experimentally.

Complex 10: [Pt(N$_3$)$_2$(OH)$_2$(Py)(3-pic)]

For complex **10**, *Table 8* shows the platinum formed distances also presenting the same behavior as for the remaining complexes to which on its singlet state difference on bond distances is not significant even orientation is different. On first conformation, N-cyclic ligands are in the same direction tending to align to hydroxyl ligand plane. And on the second conformation only pyridine is still aligned and presents definitely different azide orientation. Complex conformations are presented on *Table 7*.

Singlet ground State	
Conformation 1	Conformation 2
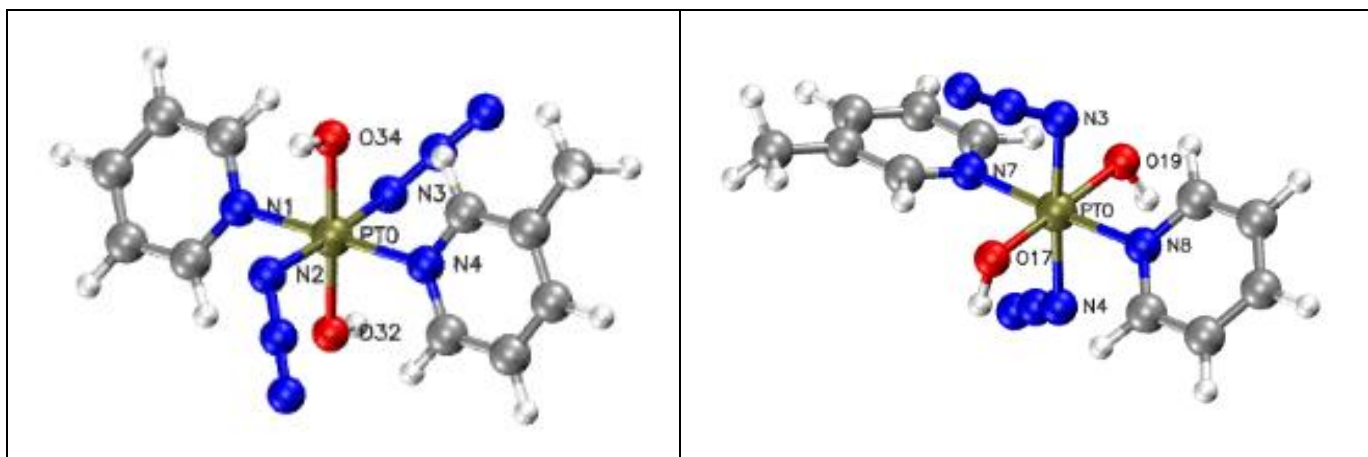
Table 7: Complex 10: Trans,trans-[Pt(N$_3$)$_2$(OH)$_2$(3-picoline)(py)] complex conformations.

	Singlet ground State	Triplet ground State
Conformation 1		
PT-N1	2.0239	2.362
PT-N4	2.0403	2.041
PT-N3	2.0548	2.424
PT-N2	2.0519	2.051
PT-O32	2.0022	2.005
PT-O34	2.0027	1.985
	Singlet ground State	Triplet ground State
Conformation 2		
PT-N7	2.0459	2.0567
PT-N4	2.0612	2.4351
PT-N3	2.0462	2.3802
PT-N8	2.0210	2.0625
PT-O17	2.0014	1.9854
PT-O19	2.0080	1.9651

Table 8: Complex 10: Trans,trans-[Pt(N$_3$)$_2$(OH)$_2$(3-picoline)(py)] complex bond distances of each conformation

N$_3$-Pt bond distances elongation on previously discussed complexes is a feature of almost all complexes conformations, even though two conformations do not show the same behavior and so on will be studied to understand influence of azide orientation among other on its triplet state geometry. Despite, O-Pt distances on **7,8** complexes tend to decrease on their triplets' geometry due there is not a critical steric factor, **9,10** O-Pt bond distances slightly increase or its decrease is minimum due they present double pyridine and a steric methyl group compared to **7,8** complexes. Only **8** and **9** second conformation triplets' geometries do not show this behavior due elongation its placed on amine derived ligands instead on azide ligand.

IV.2.2 Electronic properties
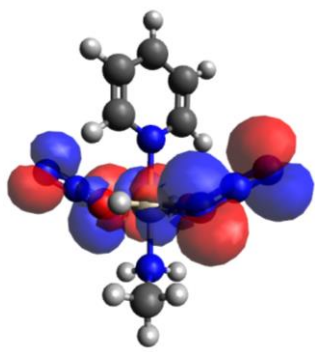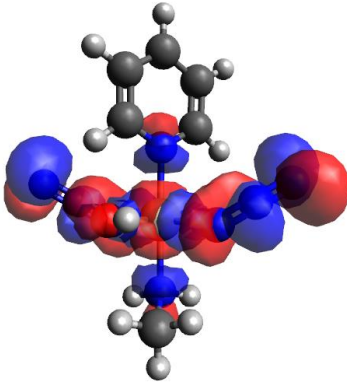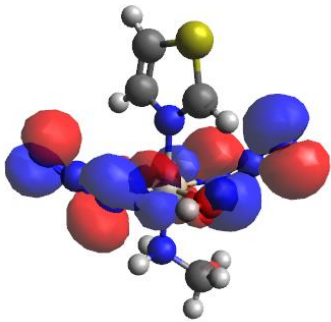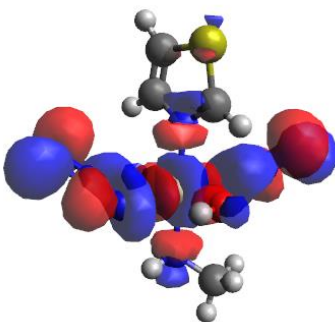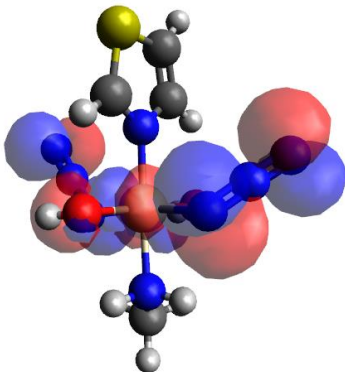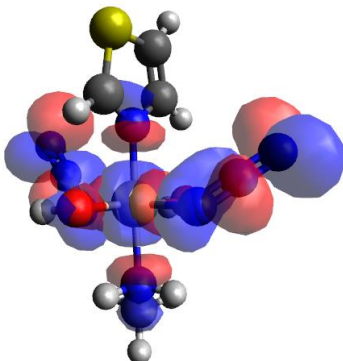
Mulliken partial charges for platinum atoms were obtained from singlet and triplet geometries.
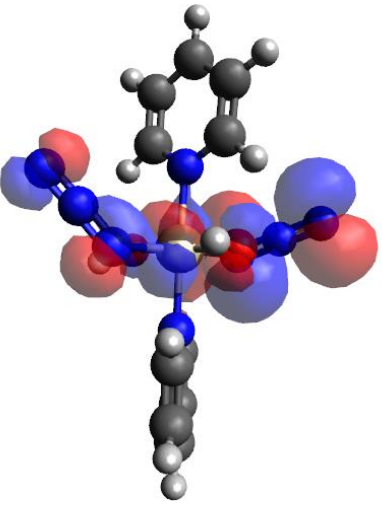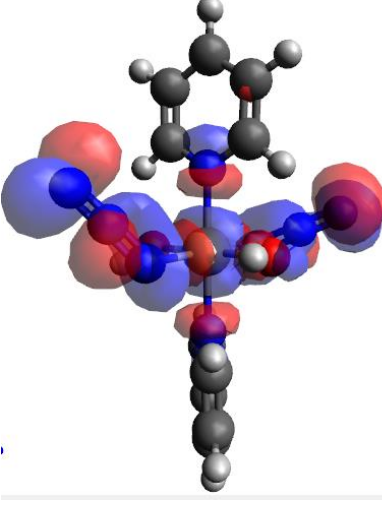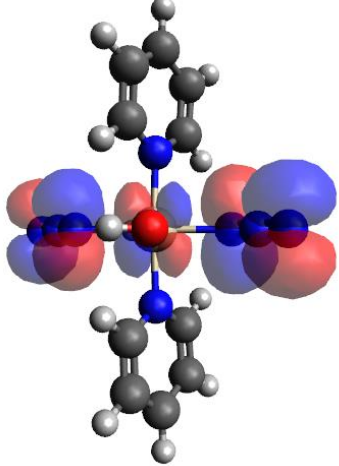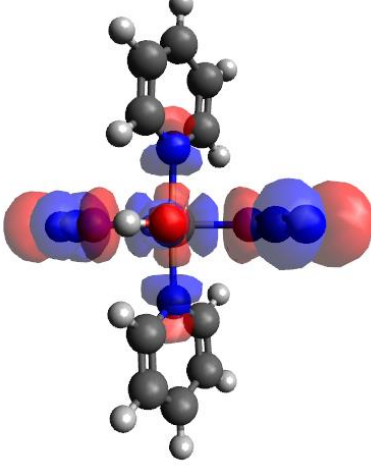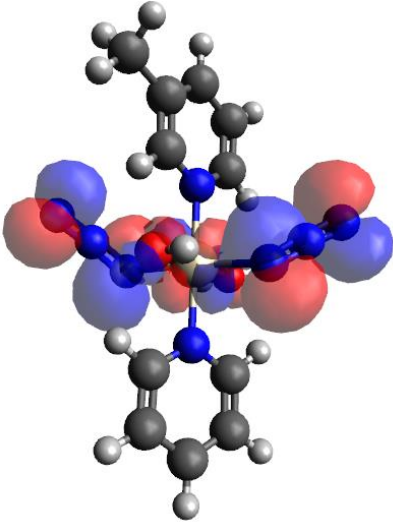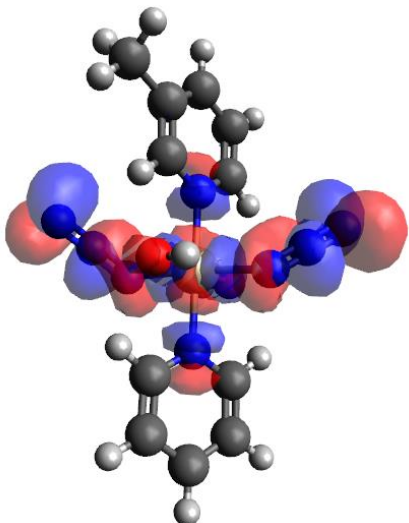
Mulliken Platinum Charges		
	Singlet	Triplet
7.1	0.771	0.671
7.2	0.834	0.673
8.1	0.791	0.910
8.2	0.760	0.534
9.1	0.728	0.582
9.2	0.760	0.886
10.1	0.709	0.584
10.2	0.732	0.552

Table 9: Mulliken charges

A correlation is seen that when changing of amine derived ligands a decrease on positive charge on platinum is observed and same character is presented on its triplets' state. Also for each complex, when comparing the most stable singlet with the most stable triplet, a decrease of positive charge on triplets' states is observed and could be correlated to the reduction of $Pt^{(IV)}$ to $Pt^{(II)}$. Same behavior is seen between complexes conformation with two particular cases, **8** and **9** second conformation triplets' states does not show a decrease of positive charge meaning that their platinum reduction is not favored.

HOMO and LUMO orbitals of complexes		
Complex	HOMO orbital	LUMO orbital
7.1		

7.2		
8.1		
8.2		

9.1		
9.2		
10.1		

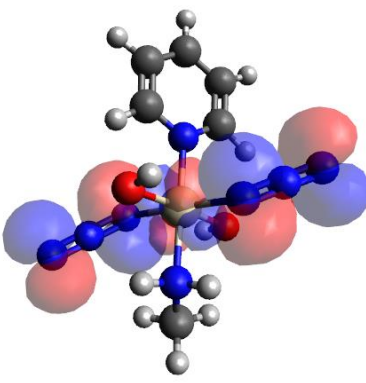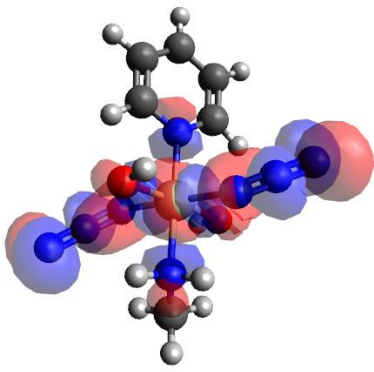| 10.2		

Table 10: Complexes HOMO and LUMO orbitals

Each complex has some differences in their electronic properties due to the ligands used, suggesting a different reactivity. The photo-reactivity, involving electronic transitions induced by light, is discussed in the following part.

IV.2.3   Summarize of differences between complexes 7, 8, 9 and 10

For **7** complexes conformations, the second conformation presents Mulliken charge greater, so to achieve this charge difference to reduce the metal could be more difficult and more energetic transitions may be necessary to reduce platinum on second conformation compared to first conformation. Same idea could be fit on each complex, instead there are two conformations that does not reduce platinum charge, so in this case reduction of platinum is not favored and it is related that not azide release is expected on triplet state, making in this way azide principal responsible of reducing the metal.

IV.3   Singlet to singlet transitions and spin–orbit allowed transitions calculated in TDDFT as a tool for estimating the reactivity

After calculating the structures of the potential anti-cancer complexes and highlighting their differences in electronic properties, this part is focused on deciphering their photo-reactivity. As exposed in the theoretical framework part, platinum complexes can exhibit a peculiar reactivity while exposed to light through electronic transitions (singlet-singlet or singlet-triplet caused by SOC).
Singlet excited states for complexes **7,8,9,10** were calculated, generating a UV-VIS spectrum in which for each one, transitions responsible for their activation will be explained.

SOC contribution is calculated between excited singlet states with spin adapted triplets (closest triplet state for S1). On previous study of Ir(ppy)3 complex, it was concluded that the geometry corresponding to emitting species is an intermediate form between singlet ground state and triplet excited state geometries, although an accurate approach to obtain results comparable with the experimental ones is based on the singlet ground optimized geometry. [38] Due to this, SOC contribution was calculated using molecule coordinates previously generated by geometry singlet optimization.

IV.3.1 Complex 7

Simulated UV-Vis spectrum using TDDFT method
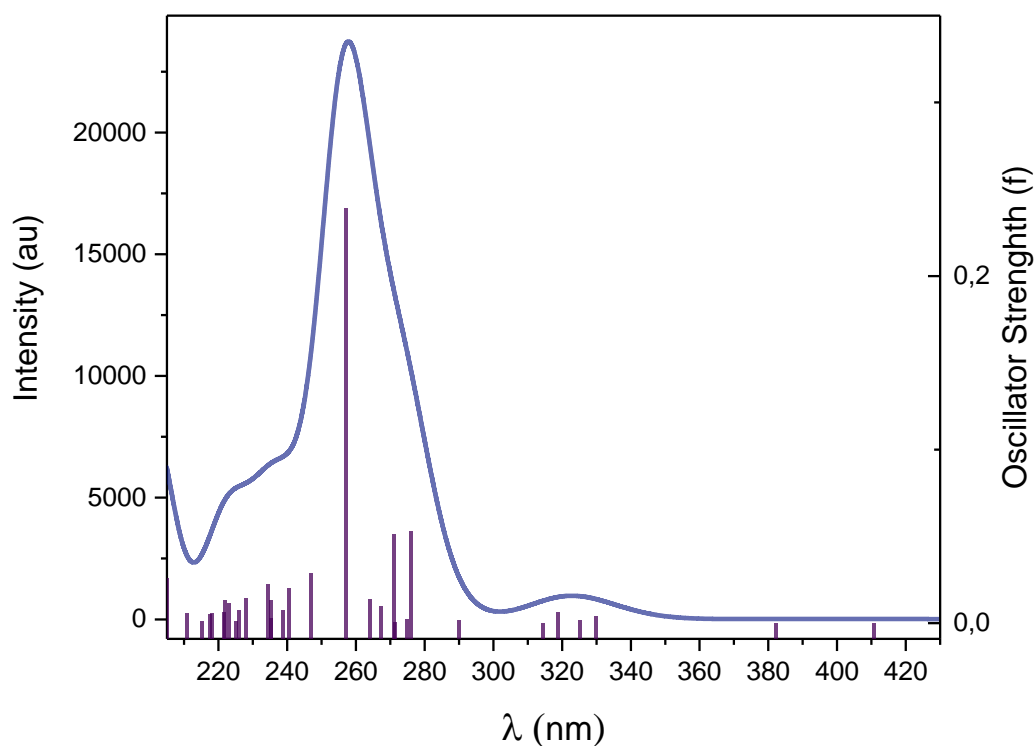
Figure 10 Theoretical UV-VIS spectrum of complex **7**(conf.1).

State	Energy (eV)	Wavelength (nm)	Major Contributions	Oscillator Strength
1	3.019	410.7	HOMO → LUMO (97%)	0.00012
2	3.243	382.3	HOMO-1 → LUMO (98%)	0.00008
3	3.767	329.9	HOMO -2 → LUMO (94%)	0.00387
4	3.941	314.6	HOMO-1 → LUMO+2 (52%) HOMO-1 → LUMO+3 (44%)	0.00007
5	3.812	325.3	HOMO → LUMO+1 (90%)	0.00186

6	4.275	290.0	HOMO-5 → LUMO (20%) HOMO-4 → LUMO(10%) HOMO → LUMO+2(43%) HOMO → LUMO+3(10%)	0.00182
7	3.891	318.7	HOMO-1 → LUMO+1(93%)	0.00649
9	4.695	264.1	HOMO-6 → LUMO(35%) HOMO-5 → LUMO(16%) HOMO-4 → LUMO(38%)	0.01391
10	4.822	257.1	HOMO-3 → LUMO(52%) HOMO-2 → LUMO+1(10%) HOMO → LUMO+3(12%)	0.23896
11	4.494	275.9	HOMO-3 → LUMO(10%) HOMO-2 → LUMO+1(84%)	0.05296
18	5.292	234.3	HOMO-8 → LUMO(13%) HOMO-7 → LUMO(52%) HOMO-2 → LUMO+2(13%)	0.02234
28	5.586	221.9	HOMO-6 → LUMO+1(27%) HOMO-3 → LUMO+2(9%) HOMO-3 → LUMO+3(48%)	0.01324

Table 11: TDDFT calculation for complex **7**(conf.1)

It was reported that experimentally the maximum absorption peak for complex **7** is at 289nm while in our theoretical spectrum the most intense band corresponds to the transition at 257.1nm. Such transition present major contribution from orbitals that involves LMCT/IL charge transfer showing dissociative character on N_3-Pt bond. Furthermore, its oscillator strength value (*f*) represents the most probable transition. Information of transitions of theoretical transitions for first conformation is seen on *Table 11*.

UV nearest transitions with high *f* values present more dissociative character on OH-Pt bond than theoretically N_3 release, explaining that azide release is activated at a longer wavelength and is the reason why after irradiation band at approx. 235nm increases due to OH ligand is still present. Unlike the most intense band where almost all contribution goes to LUMO orbital decreases due to antibonding interaction between azide and platinum is significant, and with irradiation this interaction disappears as azide ligand.

Taking as a reference the shift difference between experimental and theoretical spectra which is seen on *Figure 10*, transitions that were assigned experimentally to azide release could also be shifted. The less energetic transition obtained in TDDFT calculation is at 410.7nm, corresponding to a transition from HOMO to LUMO orbital which presents a dissociative LMCT character (strong-N_3→Pt/weak-

OH→Pt) and d-d transitions. Bearing in mind that the most probable transitions, more intense, have higher oscillator strength, it is expected that the most probable transitions are in the UV region. Theoretically higher oscillator strength value after 200nm was determined at 234.3nm, which arises from a major contribution of LMCT/IL charge transfer related to the strong and weak dissociative character of OH and azide ligand, respectively.

SOC contribution to transitions

Even though transitions are present in the visible region, they do not account for the experimental behavior of complex **7** beyond 400nm irradiation. A hypothesis could be that if triplet states could be reached after excitation, some new transitions could appear in the visible region, which would not appear on the simulated UV-VIS spectrum due to the selection rules of this spectroscopy. Based on this hypothesis, and knowing that reaching triplet states could be allowed by spin-orbit coupling, it must be kept in mind the relation of SOC contribution with Z value: SOC contribution increases as the atomic number Z increases, which influence is proportional to Z^4.[45]

Consequently, SOC contributions on the transitions and the spectrum were calculated. The new spectrum in *Figure 11* includes corrections where there is intersystem crossing reaching triplets states which contribute to different transitions. The SOC contributions induce a differential displacement of wavelengths for different transitions, generating a different graph.

In this spectrum, a higher number of transitions are present in the visible region. The vast majority of SOC states reached are not purely singlet or triplet but rather present a hybrid character. Interestingly, most red-shifted transitions present almost all components their as triplets. It is also worth noting that not only one triplet is involved in these transitions but a mixture of triplets T_1 and T_2. Indeed, the most right-shifted transition at 445.4nm is only conformed by triplet states with 49% of T_1 state contribution and 43% of T_2 state contribution. This type of transition can only appear when taking into account SOC contributions and was logically absent from the previous simulated UV-Vis graph where this type of transition is normally forbidden.

The most red shifted singlet state occurs in the previously calculated spectrum at 410.7nm; which compared with SOC spectrum values could be attributed at 420.6nm. Based on SOC corrected data (*Table 12*), this state has the major contribution coming from singlet state (S_1) around 410nm wavelength. Even though triplet states contribution is more significant, amounting for 79% of the contribution, the singlet state S_1 amounts for 17% of the contribution. The wavelength shifting is

significant due to the fact that the triplet states involved correspond to low triplet states, consequently, that will lead the transition to a lower (Visible region) energy level. Owing to the hybrid states contribution in SOC calculated transitions explains why is not possible to determine shifting factor between TDDFT and SOC contribution.

Considering triplet transitions only, both transitions on the visible region present a strong dissociative character of N_3-Pt bond and a less intense dissociative character of the OH ligand. The most intense absorption band obtained in SOC spectrum is at 248.9nm and relates to the previously calculated at 257.1nm (singlet transitions only), showing a shift towards the UV region. Despite that this transition contains 27% of triplet states contribution, their level of energy goes from a T_{15} to T_{25} states, which are highly energetic, making the transition energy more UV shifted. It can be concluded that triplet states population in this complex influence the transitions in different manner, where the crucial factor on the wavenumber shift depends on the energy level of the triplet states involved.
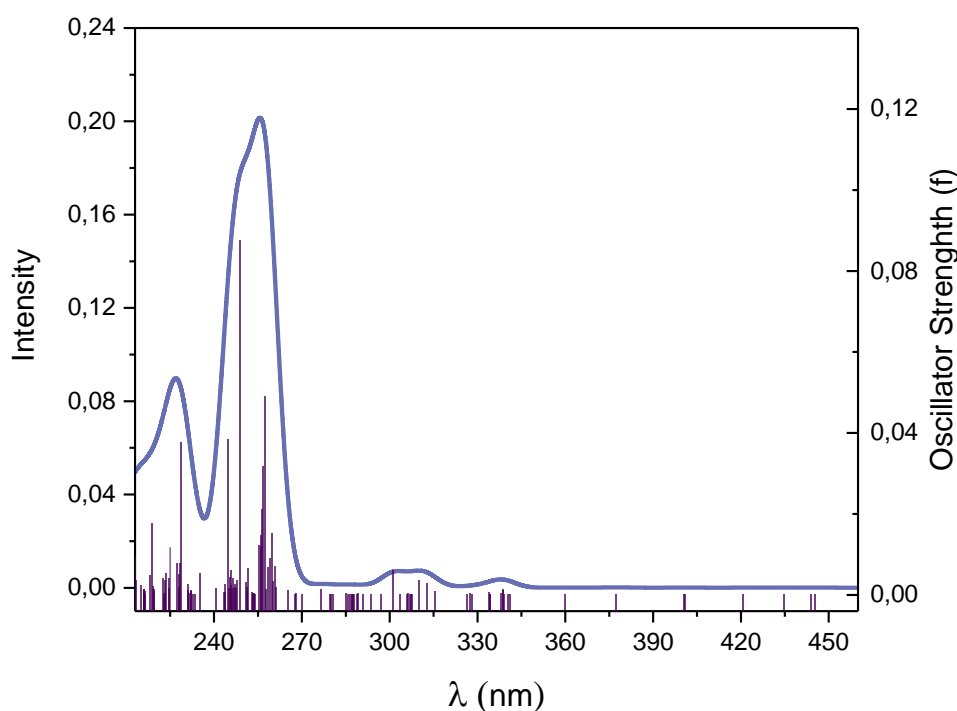
Figure 11 SOC contribution for complex **7**(conf.1)

SOC Contribution				
State	Energy (cm-1)	Wavelength (nm)	Oscillator Strength	Spin Contribution

1	22453.3	445.4	0.00002	T_1 (51%) T_2 (42%)
2	22528.8	443.9	0.00003	T_1 (73%) T_2 (23%)
3	23011.9	434.6	0.00004	S_2 (4%) T_1 (90%) T_6 (1%)
4	23775.7	420.6	0.00001	S_1 (17%) T_2 (77%)
5	24939.3	401.0	0.00001	T_1 (25%) T_2 (70%)
6	24958.8	400.7	0.00002	T_1 (23%) T_2 (72%)
7	26505.1	377.3	0.00015	S_1 (78%) T_2 (17%)
8	27795.9	359.8	0.00003	S_2 (87%) T_1 (7%)
12	29508.5	338.9	0.00123	T_3 (94%)
74	40171.9	248.9	0.08759	S_{10} (63%) T_{34} (3%) T_{16} (14%)

Table 12: SOC contribution of complex 7 (conf.1)

Effect of the conformation on the transitions

Further TDDFT of second conformation of complex **7** was calculated, giving a slightly different spectrum. The difference of energy between two conformations is quite small to establish one more favorable than other. Due to this also SOC contribution is calculated, aiming a more accurate relation to experimental behavior and establish a more accurate conformation.

Figure 12 Theoretical UV-Vis spectrum of complex **7**(conf.2)

State	Energy (eV)	Wavelength (nm)	Major Contributions	Oscillator Strength
1	3.194	388.2	HOMO → LUMO (95%)	0.002130
2	3.241	382.6	HOMO-1 → LUMO (97%)	0.000076
3	3.388	365.9	HOMO-2 → LUMO (94%)	0.001347
5	3.811	325.3	HOMO-1 → LUMO+1 (78%) HOMO→ LUMO+1 (20%)	0.004448
7	3.999	310.0	HOMO-2 → LUMO+1 (98%)	0.001085
8	4.456	278.2	HOMO → LUMO +2(12%) HOMO → LUMO+3 (75%)	0.002120
11	4.710	263.2	HOMO -5→ LUMO(31%) HOMO -4→ LUMO(51%) HOMO-3 → LUMO (10%)	0.045852
12	4.831	256.6	HOMO-5 → LUMO (10%) HOMO-3 → LUMO (53%)	0.240770
15	4.585	270.4	HOMO-1 → LUMO+2 (47%) HOMO → LUMO+2 (35%)	0.005234
18	5.270	235.3	HOMO-8 → LUMO (33%) HOMO-7 → LUMO (32%) HOMO-3 → LUMO (10%)	0.111896
21	5.458	227.2	HOMO-8 → LUMO+2 (9%) HOMO-4 → LUMO+1 (72%)	0.029555

Table 13: TDDFT results of complex **7**(conf.2)

SOC Contribution			
State	Energy (cm-1)	Wavelength (nm)	Oscillator Strength	Spin Contribution

State	Energy (cm-1)	Wavelength (nm)	Oscillator Strength	Spin Contribution
1	23130.14	432.3	0.000026	T_1 (34%) T_2 (47%) T_3 (14%)
2	23404.6	427.3	0.000045	S_3 (3%) T_1 (41%) T_2 (51%)
3	23693.3	422.1	0.000119	S_1 (7%) T_3 (16%) T_2 (70%)
4	23945.2	417.6	0.000881	S_2 (8%) T_3 (14%) T_1 (72%)
7	26157.3	382.3	0.000206	S_2 (5%) T_3 (70%) T_1 (20%)
10	27796.1	359.8	0.002287	S_1 (86%) T_3 (5%)
77	39908.5	250.6	0.044140	S_{11} (80%) T_{16} (9%)
112	44437.3	225.0	0.034584	S_{18} (20%) S_{19} (9%) T_{26} (62%)

Table 14: SOC contribution for complex **7**(conf.2)

Compared to conformation 1 of complex **7**, allowed transitions obtained from TDDFT calculations (*Table 13*) has been shifted to UV region and also its point obtained at SOC contribution(*Table 14*). No transitions are present above 400nm, the most closer transitions are at 388.2, 382.6, and 365.9nm which involves major contribution transitions that go from HOMO, HOMO-1, HOMO-2 to a LUMO orbital, respectively. LUMO orbital as for complex **7** config.1 presents a strong dissociative character to azide ligand and weak dissociative character for OH and amine derived ligands. The most intense transition is still present at the same wavelength, 256.6nm where major contribution reaches LUMO orbital and according to experimental this band decreases after light exposure because most significant interaction at this orbital involves azide-platinum antibonding character. As well as a transition with a high oscillator strength value is pointed at 235.3nm, which involves major contribution leading to LUMO orbital. SOC corrected values achieve as maximum point 432.3nm where all contribution comes from a hybrid triplet character. SOC values are correlated with value reported at TDDFT calculations, due triplets' states generated are close to a singlet state.

Compared between two configurations, on LUMO+4 orbital of both, there is a big orbital involving azide with MA ligand which are related that azide interacts with orbitals that are responsible of back bonding character diminishing doubling of the octahedral field. This character is seen for both so an explanation why conformation one absorbs at higher wavelength is the energy of this interaction and interaction of remaining azide. This azide orbital is seen that can overleap also with pyridine, if more interactions are generated to ligands that involves back bonding will decrease energy of the octahedral field, making gap energy smaller and leading to transitions of being possible at longer wavelengths. Based on this, the reason why first conformation absorbs at longer wavelength could be related to azide direction, presenting different direction making more favorable the interaction with two derived amine ligands instead of one as conformation 2.
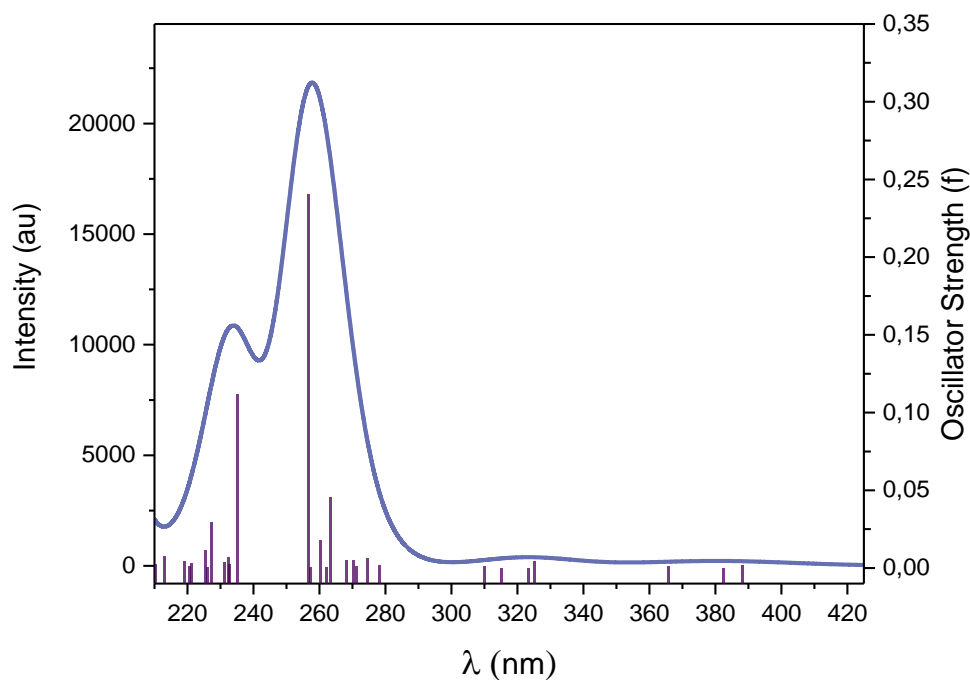
IV.3.2   Complex 8
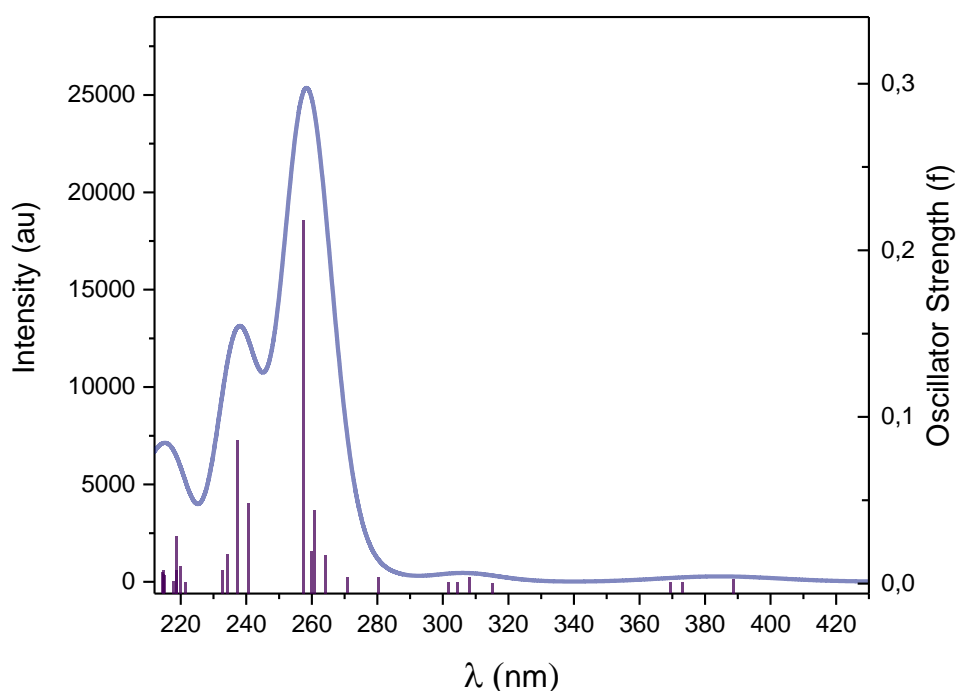
Figure 13 Theoretical UV-Vis spectrum of complex **8**(conf.1)

State	Energy (eV)	Wavelength (nm)	Major Contributions	Oscillator Strength
1	3.189	388.8	HOMO → LUMO(95%)	0.0025
2	3.324	373.0	HOMO-2 → LUMO(30%) HOMO-1 → LUMO(66%)	0.0006

3	3.357	369.4	HOMO-2 → LUMO(65%)	0.0005
5	4.026	308.0	HOMO-1 → LUMO+1(6%) HOMO → LUMO+2(83%)	0.0036
6	4.422	280.4	HOMO → LUMO+2(75%)	0.0037
11	4.750	261.0	HOMO-6 → LUMO(19%) HOMO-5 → LUMO(38%) HOMO-4 → LUMO(13%) HOMO-3 → LUMO(11%)	0.0443
12	4.814	257.6	HOMO-7 → LUMO(11%) HOMO-4 → LUMO(11%) HOMO-3 → LUMO(49%)	0.2184
15	5.227	237.2	HOMO-8 → LUMO(15%) HOMO-7 → LUMO(15%) HOMO-3→ LUMO+1(49%)	0.0860

Table 15: TDDFT results for complex **8**(conf.1)
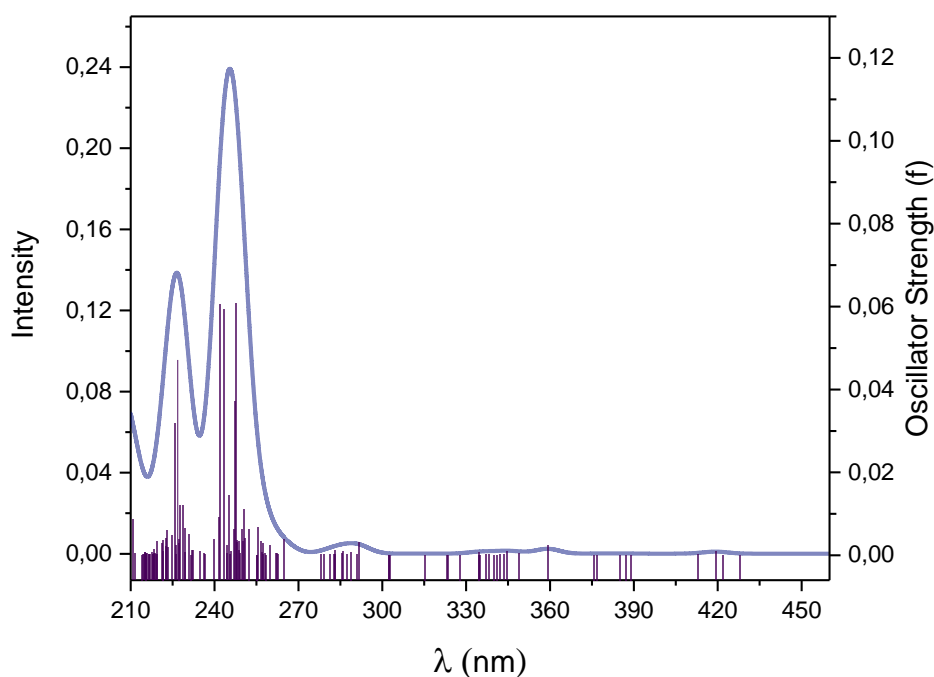
Figure 14 SOC contribution for complex **8**(conf.1)

SOC Contribution			
State	**Energy (cm-1)**	**Wavelength (nm)**	**Oscillator Strength**	**Spin Contribution**
1	23363.8	428.0	0.00001	T_1 (49%) T_3 (24%) T_2 (20%)
2	23693.4	422.1	0.00002	S_2 (2%) S_3 (1%)

				T_1 (65%)
				T_3 (21%)
3	23842.2	419.4	0.00095	S_2 (3%) S_3 (2%) T_2 (13%) T_1 (72%)
4	24221.3	412.9	0.00010	S_1 (9%) T_2 (36%) T_3 (48%)
6	25820.8	387.3	0.00004	S_2 (1%) T_3 (59%) T_1 (32%)
9	26616.8	375.7	0.00004	T_2 (55%) T_3 (36%)
10	27836.1	359.2	0.002378	S_1 (84%) T_2 (4%) T_3 (4%)
21	29571.7	334.8	0.000663	T_4 (99%)
29	34269.9	291.8	0.003055	S_5 (60%) T_5 (4%) T_8 (27%) T_9 (4%)
41	37754.1	264.9	0.003881	S_6 (76%) T_{14} (10%)
52	39143.9	255.5	0.006719	S_{11} (1%) S_{13} (1%) T_{21} (90%)
57	39896.23	250.7	0.011110	S_9 (4%) S_{12} (2%) T_{12} (10%) T_{15} (30%) T_{16} (26%)

Table 16 SOC contribution for complex **8**(conf.1)

Simulated UV-Vis spectrum using TDDFT method

As for complex **7**, which contains pyridine instead of thiazole ligand, complex **8** also shows experimentally a maximum absorption at 289nm. Theoretically, the maximum absorbance is at 257.6nm, which contains as major contribution the transition from a HOMO-3 → LUMO, representing a LMCT transition with a strong dissociative character of N_3-Pt bond and a weak antibonding interaction with amine ligands and hydroxyl ligands. Owing to the displacement between experimental and theoretical values, a hypsochromic shift could be attributed to the theoretical spectrum.

Near to the visible region, the most permitted singlet-singlet transition is at 388.8nm (*Table 15*). Major contribution at this wavelength is from HOMO → LUMO that involves a dissociative character of N_3, as well as a weak dissociative character of OH ligand. Closely energetically-related transitions involve major contribution pathways that goes from HOMO-2 and HOMO-1 to LUMO orbital that are LMCT/IL charge transfer favoring a dissociative character. Based on reported experimental results, these could be attributed to activation of the drug at 365nm, transition that will also present a hypsochromic shift.

For this complex, there is no allowed transition, singlet to singlet, in the visible region. Experimentally, this complex requires less activation time than the one previously analyzed (**complex 7**). Knowing that these 2 complexes only differ by the sulfur atom, it should be the principal responsible for this effect. Considering that the excitation to LUMO orbital brings the major contribution to drug activation, must be taken account that electron density takes place on sulfur atom implying it withdraws electronic density affecting inductive character that minors punctual splitting energy of metal making easier to put electrons on e_g orbital.

SOC contribution on transitions

As observed in the case of complex 7, spectra accounting for SOC contributions display more transitions in the visible range (*Table 16*). The singlet-singlet transition observed previously at 388.8nm is shifted to 412.9nm. For this transition, 84% of contributions comes from triplet states while 9% comes from the original singlet near 388nm. The high percentage of contribution coming from triplet states is the reason why the transition is displaced when compared to the singlet-singlet transition.

States with entirely triplet contributions are more shifted towards the visible range at higher wave numbers. This conclusion is in agreement with the previous statement that establishes that more triplet contribution there is, the more red-shifted would be the transition. It is associated with its hybrid character, transitions at 375.7nm and 334.8nm demonstrates that even having all contribution form triplet states are UV shifted due energy levels of its triplet state. Explaining this, mentioned SOC states require more energy to reach higher energy levels.

The most red-shifted transition at 428.0nm, 422.1nm, 419.4nm and 412.9nm are potentially the ones which could explain the experimental activation of the complex. However, the experimental value for the complex activation is actually reported at longer wavelength. This fact was the main motivation

for searching for another conformation which could produce transitions at higher wavelength. Almost all these transitions present an entire population of triplet states, except the transition at 412.9nm discussed before which present a singlet contribution of 9%.

The second conformation for complex **8** possess an orientation of azide and methylamine ligands equivalent to the second conformation of complex **7**, aiming to gain a better understanding through modifying only one parameter.

Effect of the conformation on the transitions

Considering that complex **8** presents two conformations with a small energy difference (<5 kJ/mol), no clear evidence of which is more favored can be established. TDDFT calculation was carried for the second conformation of complex **8**.
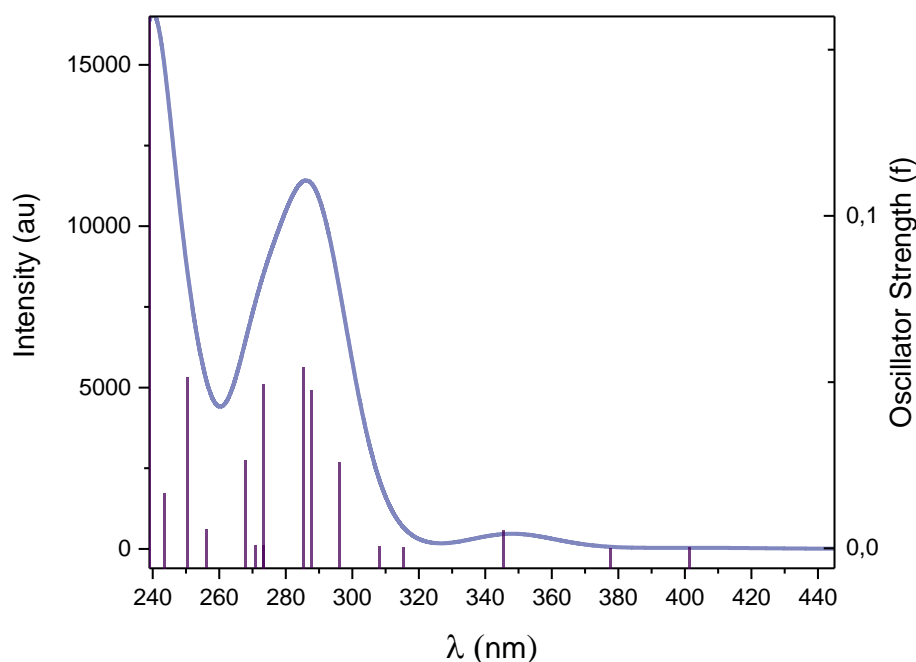
Figure 15 Theoretical UV-Vis of complex **8**(conf.2)

State	Energy (eV)	Wavelength (nm)	Major Contributions	Oscillator Strength
1	3.059	405.3	HOMO → LUMO(97%)	0.0003
2	3.253	381.1	HOMO-1 → LUMO(98%)	0.0001
3	3.562	348.1	HOMO-2 → LUMO(88%)	0.0054
4	3.909	317.2	HOMO-1 → LUMO+2(93%)	0.0002

6	4.328	286.5	HOMO-3 → LUMO(22%) HOMO → LUMO+1(28%) HOMO → LUMO+2(31%)	0.0545
7	4.168	297.5	HOMO-5 → LUMO(4%) HOMO-3 → LUMO(8%) HOMO → LUMO+1(70%) HOMO → LUMO+2(11%)	0.0257
10	4.525	274.0	HOMO-5 → LUMO(16%) HOMO-4 → LUMO(68%) HOMO-3 → LUMO(9%)	0.0493
13	4.945	250.7	HOMO-6 → LUMO(37%) HOMO-5 → LUMO+2(3%) HOMO-2 → LUMO+2(40%)	0.0515

Table 17 TDDFT results for complex **8**(conf.2)

SOC Contribution			
State	**Energy (cm-1)**	**Wavelength (nm)**	**Oscillator Strength**	**Spin Contribution**
---	---	---	---	---
1	22705.3	440.4	0.00011	T_1 (64%) T_2 (30%) T_3 (2%)
2	22789.2	438.8	0.00018	T_1 (69%) T_2 (28%)
3	23237.5	430.3	0.00013	S_2 (5%) T_1 (90%)
4	23871.7	418.9	0.00007	S_1 (15%) T_2 (75%)
5	25173.6	397.2	0.00005	T_1 (30%) T_2 (68%)
7	26882.2	372.0	0.00026	S_1 (67%) T_2 (21%) T_3 (9%)
13	28263.7	353.8	0.00058	S_2 (4%) T_{11} (90%)
18	29243.2	342.0	0.00064	T_4 (95%)
22	30855.8	324.1	0.00329	S_3 (57%) T_{10} (35%)
36	34918.5	286.4	0.00668	S_7 (8%) T_8 (77%)
39	35610.0	280.8	0.01576	S_4 (1%) S_7 (80%) T_8 (10%)
40	36318.7	275.3	0.03534	S_5 (73%) T_9 (10%)
54	38843.6	257.4	0.015423	S_{10} (38%) T_{12} (10%) T_{14} (31%) T_{16} (13%)

Table 18 SOC contribution for complex **8** (conf.2)

Second conformation transitions present a slight shift, changing its longer wavelength to 405.3nm (*Table 17*). Transition at 405.3nm presents a dissociative character with all six ligands but a remarkable stronger dissociative interaction between azide and platinum. More red-shifted transitions reach LUMO orbital, which present behavior previously mentioned. Transitions going to the UV region increase contributions that reach LUMO+2 orbital, which presents a strong dissociative character to hydroxyl and amine ligands, due drug must be able to become active at more red-shifted energy points where only azide release could be expected experimentally.

Experimentally band at 298nm decreases when it is irradiated, transitions that contribute to the formation of this band are predominantly dominated by LMCT transitions reaching LUMO orbital, leading us to know that after light exposure these transitions are not possible due azide release. It also was observed that band smaller at approx. 250nm is increased after light exposure, and this behavior could be related to the theoretical transition that takes place at 250.7nm, which presents as major contribution transitions that get to LUMO+2 orbital, presenting and intense interaction with hydroxyl and amine ligands leading us to know that these ligands are still present after light exposure.

Experimentally a more intense decrease of the band at 298nm is related to using less energetic irradiation, achieving the more considerable decrease after light exposure at 450nm; this could not be explained with the transition at 405.3nm, due this SOC contribution is calculated to aim an explanation of this behavior. Results of SOC contribution gave the possibility of new energy points for the activation of the drug. Transitions above 400nm present as major contributions which ones coming from triplets' states. Transition at 405.3nm is shifted to transition at 418.9nm, and its big shift could be related to the remaining contribution that comes from low energy triplet states that make this transition more red-shifted. The transition that was present on the previously spectrum at 250.7nm now is shifted to 257.4nm, that owns a contribution of 38% from singlet states; even major contribution comes from a triplet states the little shift is related to high energy levels of triplets (*Table 18*).

Finally, comparing two conformation spectrums with the experimental one, the second conformation spectrum presents a more accurate approach showing more clearly transitions that could be associated with experimental behavior. Moreover, experimentally an increase of signal is seen near to 200nm region; this curve behavior is only seen on the second complex conformation.

Second conformation present a different orientation of methyl(MA) and azide ligands. These characteristic is the only difference making to the second conformation to absorbs at longer

wavelengths, it means that octahedral splitting has been reduced. On second conformation it seen that azide has been placed directly up to nitrogen from thiazole, in this way interaction with p semi empty orbital of nitrogen reduces back-bonding effect therefore reducing octahedral splitting.

IV.3.3 Complex 9
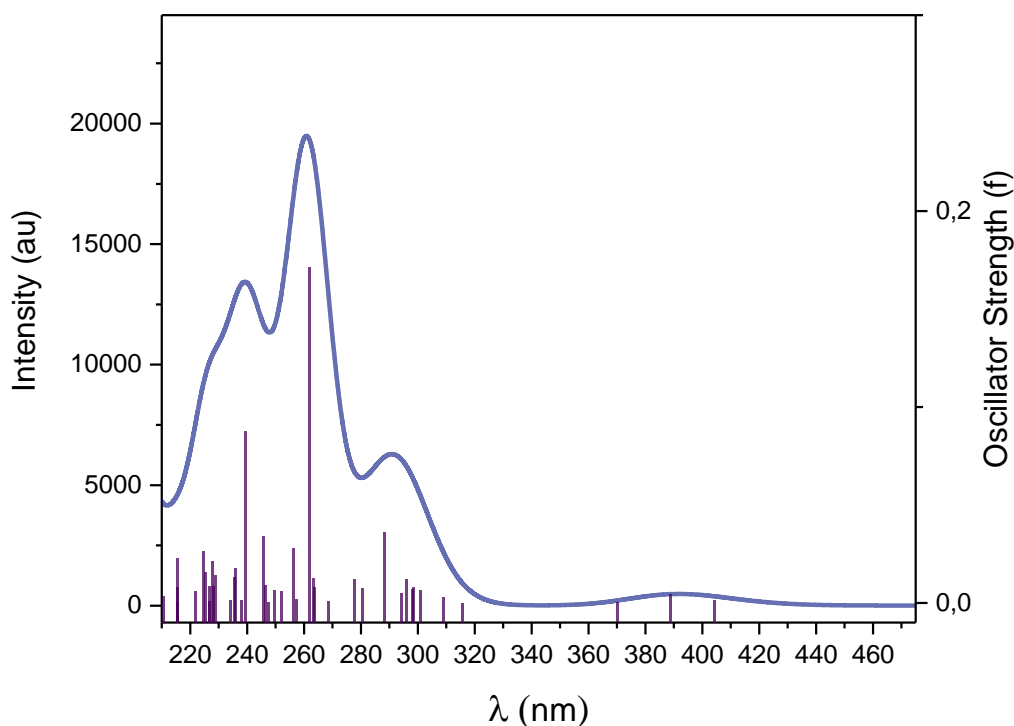
Figure 16 *Theoretical UV-Vis spectra of complex 9(conf.1)*

State	Energy(eV)	Wavelength(nm)	Major Contributions	Oscillator Strength
1	3.067	404.2	HOMO-1 → LUMO(11%) HOMO → LUMO(84%)	0.0015
2	3.188	389.0	HOMO-1 → LUMO(82%) HOMO → LUMO(11%)	0.0043
3	3.348	370.3	HOMO-2 → LUMO(98%)	0.0002
6	4.299	288.4	HOMO-6 → LUMO(10%) HOMO-5 → LUMO(18%) HOMO-4 → LUMO(22%) HOMO-3 → LUMO(22%)	0.0359
14	4.736	261.8	HOMO-4 → LUMO(25%) HOMO-3 → LUMO(32%) HOMO-8 → LUMO(9%)	0.1714
26	5.179	239.4	HOMO-8 → LUMO(8%)	0.0876

| | | | HOMO-3 → LUMO+3(17%) | |
| | | | HOMO → LUMO+5(29%) | |

Table 19 TDDFT results of complex **9**(conf.1)
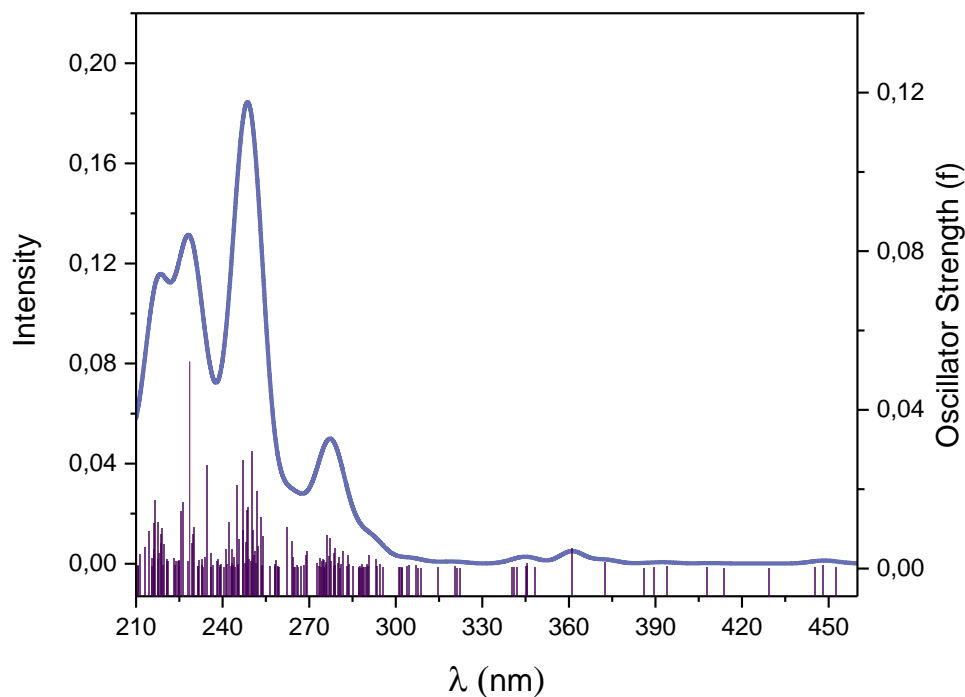
Figure 17 SOC contribution for complex **9**(conf.1)

SOC Contribution				
State	**Energy (cm-1)**	**Wavelength (nm)**	**Oscillator Strength**	**Spin Contribution**
1	22091.4	452.7	0.00035	T_1 (66%) T_2 (18%) T_3 (10%)
2	22311.6	448.2	0.00079	S_3 (2%) T_1 (77%) T_2 (16%)
3	22450.8	445.4	0.00027	S_2 (3%) T_1 (84%)
4	23293.0	429.3	0.00008	S_1 (7%) T_3 (19%) T_2 (66%)
5	24164.8	413.8	0.00007	T_2 (64%) T_1 (26%) T_3 (6%)
6	24514.3	407.9	0.00016	T_1 (22%) T_2 (70%)

7	25377.6	394.0	0.00038	S_2 (8%) T_3 (74%) T_1 (10%)
8	25681.1	389.4	0.00024	S_1 (10%) T_2 (27%) T_3 (56%)
10	26842.9	372.5	0.00155	S_1 (78%) T_3 (17%)
11	27842.9	361.1	0.004939	S_2 (84%) T_3 (12%)
85	38136.3	262.2	0.010329	S_{12} (77%) T_{15} (7%)
125	41275.5	242.3	0.0115201	S_{27} (16%) T_{33} (67%)

Table 20 SOC contribution for complex **9**(conf.1)

Simulated UV-Vis spectrum using TDDFT method

For complex **9,** the theoretically calculated spectrum is similar to the reported experimental spectrum where two representative absorption bands are found. The less energetic and more intense transition is at 261.8nm which is blue-shifted comparing to the experimental value close to 300nm. This blue-shift is also present for the more energetic but less intense transition at 239.40nm, experimentally reported at 260nm.

The band at 261.8nm corresponds to a transition where the major contribution going to the LUMO orbital, an orbital with a strong dissociative character of N_3-Pt bond and a weak dissociative character for hydroxyl and amine ligand release character. The more energetic band at 239.4nm also presents a small percentage of excitation going to the LUMO orbital (8%). However, a significant contribution comes from the transitions that reach LUMO+3, LUMO+4, and LUMO+5 orbitals that do not involve any interaction with azide ligand but instead present a strong dissociative character of OH ligand (*Table 19*).

At 404.2nm is the only transition above 400nm obtained in the simulated TDDFT spectrum, that, besides the contribution to antibonding orbital between N_3-Pt bond, presents IL charge transfer with a dissociative character of amine ligands. Through the observation of antibonding orbitals, dissociative character of hydroxide ligands is present from the orbitals LUMO+3 and onwards.

SOC contribution on transitions

Three different excitation wavelengths were used experimentally 350,420 and 450nm but did not result in pyridine release in any of the cases. Activation of the complex under 350nm irradiation could be attributed to the calculated transition at 370.3nm, in which almost all contribution presents a dissociative character of N_3 ligand. However, the fastest activation induced by a radiation at 420nm cannot be explained by solely the singlet-singlet transitions.

In this complex, SOC results give rise to additional transitions involving triplet states in the visible (*Table 20*). The highest transition in wavenumbers is at 452.7nm in which all contributions come from triplet states. As previously mentioned, the more triplet population states are present, the more red-shifted are the transitions; this effect could change depending on the energy levels of triplets compared to the singlet levels. In this case, transitions placed around and above 400nm present a high percent of triplets on low energy levels. The experimental drug activation at 420nm can be justified by the transition at 413.8nm obtained in SOC spectrum, in which all contribution comes exclusively from triplet states.

The previously mentioned transition at 404.2nm, after incorporating SOC contribution could be included in the transition at 429.nm complemented with a contribution coming from T_2 state, making this transition more red-shifted. Alternatively, the transition shifted at 394.0nm could explain the experimental observation, where a major contribution comes from the T_3 state, which is at a higher energy level than T_2 state. Most intense transitions presented in TDDFT calculation also present the highest values of oscillator strength in SOC contribution results but with a difference of intensity between two strongest transitions.

On LUMO+4 orbital there is a clear interaction between azide orbital with perpendicular orbital of pyridine with an inclination. This interaction caused the same behavior as before where it reduces back bonding character and facilitates more visible shifted transitions.

Effect of the conformation on the transitions
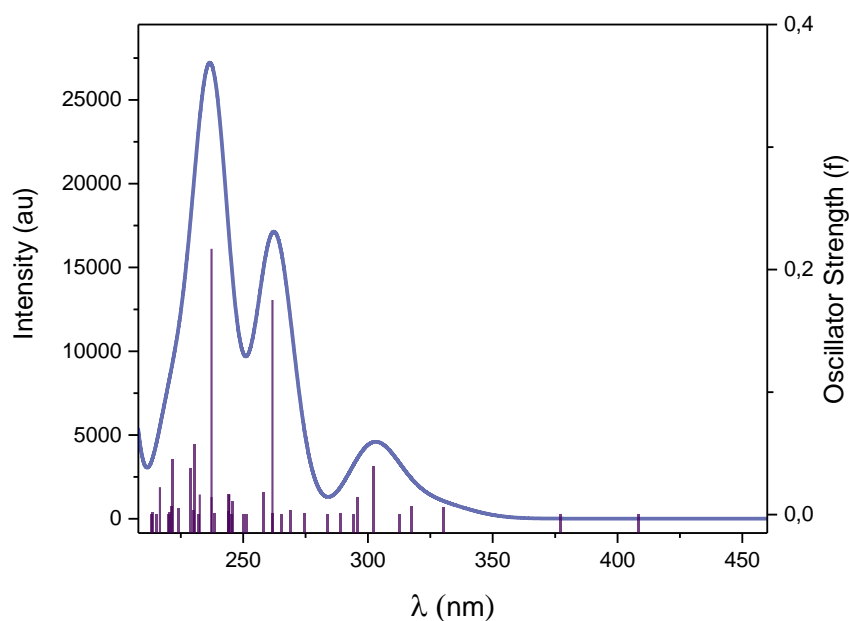
Figure 18 UV-Vis spectra of complex **9**(conf.2)

State	Energy (eV)	Wavelength (nm)	Major Contributions	Oscillator Strength
1	3.006	412.5	HOMO → LUMO (97%)	0.000001
2	3.251	381.3	HOMO-1 → LUMO (98%)	0.000036
3	3.726	332.8	HOMO-2→ LUMO (92%) HOMO→ LUMO+6 (3%)	0.005970
6	4.167	297.5	HOMO-5→ LUMO (72%) HOMO-3→ LUMO (12%)	0.014182
7	4.067	304.8	HOMO-1 → LUMO+1 (95%)	0.040839
13	4.719	262.7	HOMO-3→ LUMO (43%) HOMO → LUMO +5(31%)	0.175190
24	5.216	237.7	HOMO-5→ LUMO+3 (18%) HOMO-3→ LUMO (16%) HOMO-2→ LUMO+5 (29%)	0.216245
28	5.368	231.0	HOMO-9 → LUMO (10%) HOMO-5→ LUMO+3 (23%) HOMO-3 → LUMO+3 (29%)	0.546303

Table 21 TDDFT results for complex **9**(conf.2)

SOC Contribution				
State	**Energy (cm-1)**	**Wavelength (nm)**	**Oscillator Strength**	**Spin Contribution**
1	22563.3	443.2	0.000015	T_1 (73%)

				T$_2$ (19%)
2	22532.7	441.8	0.000010	S$_6$ (1%) T$_1$ (76%) T$_2$ (19%)
3	22840.8	437.8	0.000003	S$_2$ (3%) T$_1$ (92%) T$_6$ (1%)
4	23887.9	418.6	0.000002	S$_1$ (19%) T$_2$ (72%)
5	24947.6	400.8	0.000025	T$_1$ (18%) T$_2$ (76%)
8	27583.6	362.5	0.000056	S$_2$ (77%) T$_1$ (5%) T$_3$ (7%)
36	34709.1	288.1	0.031943	S$_7$ (82%) T$_8$ (7%)
83	39642.3	252.3	0.070087	S$_{13}$ (41%) T$_{20}$ (26%)
103	40639.5	246.1	0.059592	S$_{13}$ (11%) S$_{16}$ (4%) T$_{31}$ (30%) T$_{33}$ (38%)

Table 22 SOC contribution for complex **9**(conf.2)

If two UV-Vis spectra of two conformations are compared to experimental, a more accurate approach is obtained with first configuration due second configuration presents the most intense transition above less intense transition. More intense transitions on this complex is expected at 262.7 and 237.7nmm, in which high energy transition present a more intense character that change the shape of spectra becoming different from experimental one.

Most red-shifted transition goes from HOMO to LUMO orbital presenting the same antibonding character between platinum and azide ligand. Transition at 262.7, which on first conformation was the most intense, leads to LUMO orbital and most intense transition is 237.7nm (*Table 21*), in which major contributions shows a strong dissociative character to hydroxyl and pyridine ligands. Experimentally not pyridine release was observed, even energy difference is around 1KJ/mol, it seems that this conformation does not approach the observed behavior as experimental fitting spectra.

SOC contribution reaches as most red shifted transition at 443.0nm, presetting completely triplets' contribution (*Table 22*). Not more in deep interpretation of SOC contribution is taken account due enough complex behavior lead to know that it is not present experimentally. Instead, first conformation shows a greater SOC contribution and it could be related that azide interaction with pyridines makes

them slightly elongate withdrawing electronic density and making nucleus to be felt more positive making easier to achieve triplet stable states. This interaction is more difficult on second conformation due orientation of azides is perpendicular to pyridine direction.

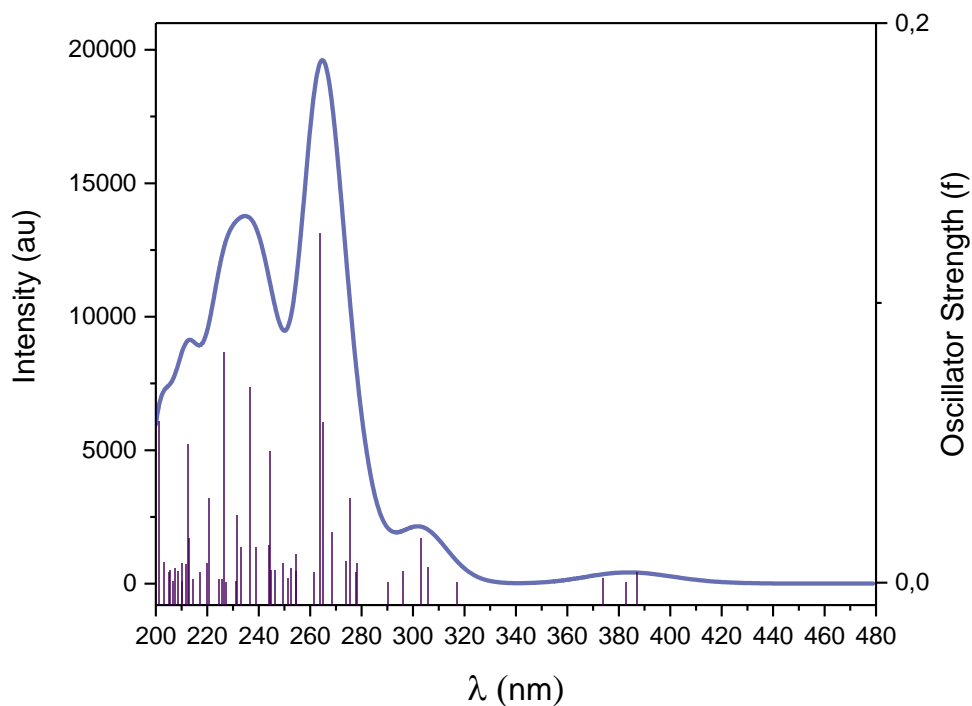*Figure 19* Theoretical UV-Vis spectra of complex **10**(conf.1)

State	Energy (eV)	Wavelength (nm)	Major Contributions	Oscillator Strength
1	3.210	386.2	HOMO → LUMO (94%)	0.003768
2	3.323	373.1	HOMO-2 → LUMO (94%)	0.001383
3	3.238	382.9	HOMO-1 → LUMO (97%)	0.000001
6	4.086	303.4	HOMO-1 → LUMO+1 (27%) HOMO → LUMO+1 (69%)	0.016880
10	4.503	275.3	HOMO-5 → LUMO (24%) HOMO-1 → LUMO+2 (11%) HOMO-3 → LUMO+2 (33%)	0.010577
15	4.699	263.9	HOMO-4 → LUMO (28%) HOMO-3 → LUMO (30%) HOMO-2 → LUMO+2 (4%)	0.109178
14	4.688	264.5	HOMO-8 → LUMO (6%) HOMO-5 → LUMO (6%) HOMO-4 → LUMO (27%) HOMO-3 → LUMO (20%) HOMO-2 → LUMO +2(8%)	0.0792545

			HOMO-2 → LUMO+3 (7%)	
26	5.285	234.6	HOMO-9 → LUMO (19%) HOMO-3 → LUMO+3 (54%)	0.0393002
31	5.472	226.6	HOMO-5 → LUMO+1 (44%) HOMO-4 → LUMO+2 (14%)	0.0826106

Table 23 TDDFT results for complex **10**(conf.1)
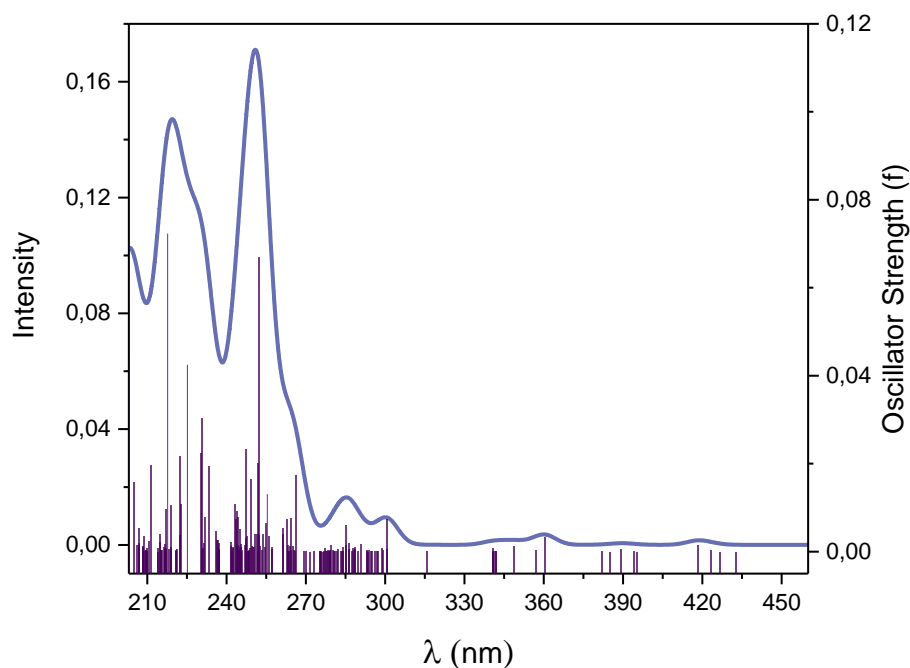
Figure 20 SOC contribution for complex **10**(conf.1)

State	Energy (cm-1)	Wavelength (nm)	Oscillator strength	Spin Contribution
1	23108.7	432.7	0.000002	T_1 (31%) T_3 (46%) T_2 (16%)
2	23432.1	426.8	0.0000006	S_2 (3%) T_1 (39%) T_3 (51%)
3	23631.4	423.2	0.00034	S_1 (5%) T_2 (23%) T_3 (68%)
4	23914.6	418.2	0.00136	S_3 (8%) T_2 (22%) T_1 (66%)
5	25307.0	395.1	0.000002	T_1 (54%) T_3 (41%)

6	25383.5	394.0	0.000064	T_1 (58%) T_3 (39%)
7	25683.4	389.4	0.00051	S_3 (2%) T_2 (67%) T_1 (28%)
9	26179.3	382.0	0.000054	T_3 (11%) T_2 (80%)
10	27749.9	360.4	0.0032	S_1 (89%) T_3 (2%) T_5 (2%)
11	28012.7	357.0	0.000400	S_3 (85%) T_2 (6%)
12	28661.2	348.9	0.001319	S_2 (91%) T_3 (1%)
14	29252.1	341.9	0.000153	S_1 (2%) S_9 (1%) T_5 (84%)

Table 24 SOC contribution for complex **10**(conf.1)

Simulated UV-Vis spectrum using TDDFT method

For complex **10**, the experimental spectrum presents two absorption bands, one less energetic band at 295nm and a more energetic but less intense band at 265nm. The theoretically less energetic band could be attributed to the transition at 263.9nm, which has a high oscillator strength and present as major contribution transition from HOMO-4, HOMO-3 bonding orbital to LUMO orbital that present a strong dissociative character between N_3-Pt bond. The more energetic experimental band could be the sum of two transitions states with great oscillator strength values, the first at 234.6 nm, where the most populate transition goes from HOMO-3 to LUMO+3 orbital presenting a strong dissociative character between hydroxyl and platinum bond *(Table 23)*. The second transition state is at 226.6nm and presents an IL charge transfer to pyridine and picole ligand without representing any dissociate character. Thus, this is reflected in the experimental results: this band does not disappear after irradiation because no dissociative character of this transition is involved, and the IL charge transfer goes to pyridine.

SOC contribution on transitions

Experimentally two wavelengths were used for drug activation, at 517 and 471.2nm which are not seen on calculated singlet excited states, so, in the same approach, SOC contribution was calculated. After SOC contribution is taken account, transitions above 400nm are found. Even contribution makes

red shifted transition goes from 386.2 to 432.7, while a significant increment, it does not reflect the experimental results (*Table 24*). Azides are oriented diagonal to picole ligand, and methyl is generating electron density so carbons responsible of back bonding metal now are back boding this electron density, so even azide presence reduces back bonding character it has already been reduced by methyl.

Establishing a new conformation, in which one azide orientation is put slightly away from picole and pyridine ligand is not aligned to OH containing plane as observed in previous complex.
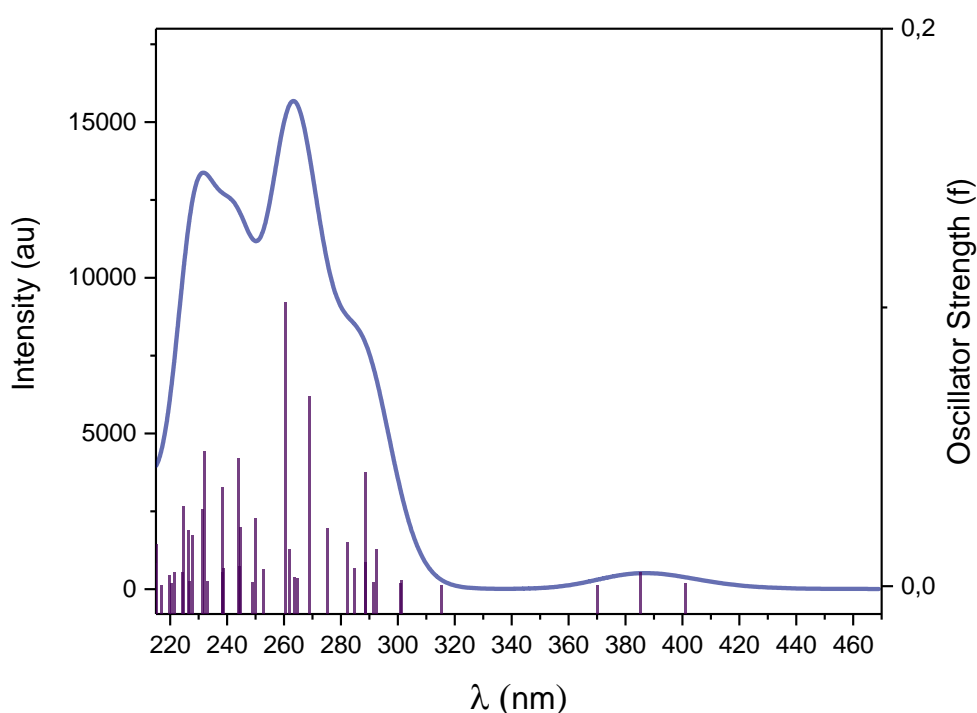
Effect of the conformation on the transitions

Figure 21 Theoretical UV-Vis spectra for complex **10**(conf.2)

State	Energy (eV)	Wavelength (nm)	Major Contributions	Oscillator Strength
1	3.089	401.3	HOMO → LUMO (87%)	0.001141
2	3.218	385.3	HOMO-1→ LUMO (83%)	0.004971
5	4.292	288.8	HOMO -6→ LUMO (33%) HOMO -5→ LUMO (11%) HOMO -3→ LUMO (26%)	0.040767
7	4.117	301.2	HOMO-1→ LUMO+1 (52%) HOMO → LUMO+1 (33%)	0.002046
12	4.506	275.2	HOMO-4 → LUMO (6%) HOMO -3→ LUMO (6%)	0.020708

			HOMO-2 → LUMO+1 (6%) HOMO -2→ LUMO+3 (17%) HOMO-1 → LUMO+3 (16%) HOMO → LUMO+3 (23%)	
14	4.609	269.0	HOMO-4→ LUMO (50%) HOMO-3→ LUMO (16%) HOMO-2 → LUMO+3 (7%) HOMO-1 → LUMO+3 (7%)	0.068190
16	4.756	260.7	HOMO-6 → LUMO (21%) HOMO-5 → LUMO (15%) HOMO-4 → LUMO (30%) HOMO -3→ LUMO(13%)	0.101722
13	4.238	292.6	HOMO-2 → LUMO+2 (71%) HOMO-1 → LUMO+2 (14%)	0.013190
28	5.347	231.9	HOMO -6→ LUMO+1 (12%) HOMO-5 → LUMO+1 (10%) HOMO-4 → LUMO+1 (38%) HOMO-2 → LUMO+5 (8%)	0.048148

Table 25 TDDFT results for complex **10**(conf.2)

SOC Contribution				
State	**Energy (cm-1)**	**Wavelength (nm)**	**Oscillator Strength**	**Spin Contribution**
1	22570.1	443.1	0.000364	T_1 (61%) T_2 (20%) T_3 (7%)
2	22818.5	438.2	0.000753	S_3 (3%) T_1 (3%) T_2 (4%) T_3 (6%)
3	22959.9	435.5	0.000368	S_2 (2%) S_3 (1%) T_1 (76%) T_2 (8%)
4	23637.2	423.1	0.000093	S_1 (9%) T_3 (27%) T_2 (58%)
5	24656.0	405.6	0.000008	T_1 (32%) T_2 (55%) T_3 (8%)
7	25513.6	391.9	0.00355	S_2 (5%) T_3 (71%) T_1 (14%)
11	27870.0	358.8	0.005695	S_2 (85%) T_3 (9%)
62	36132.5	276.8	0.016804	S_4 (1%) S_5 (37%) S_8 (4%) S_{13} (7%)

				T$_{15}$ (9%)
				T$_{12}$ (10%)
92	39000.2	256.4	0.038794	S$_{12}$ (1%)
				S$_{14}$ (70%)
				T$_{28}$ (13%)
111	40155.0	249.0	0.051512	S$_{16}$ (50%)
				T$_{23}$ (32%)

Table 26 SOC contribution of complex **10**(conf.2)

Most intense band is placed around 290nm experimentally, at theoretical spectra most intense band is at 260nm that possess the highest oscillator value and major contribution presents a LMCT/IL charge transfer with a stronger dissociative character with azide ligands. Near to this transition, another with high oscillator value present the same transition as major contribution making this band responsible for azide release. More energetic but less band observed experimentally is around 260nm that on TDDFT results could be related point at 231.9nm that presents major contributions from transitions reaching LUMO+1 orbital with IL charge transfer character. In this orbital is appreciable that bonding orbital between picole and platinum is stronger than pyridine platinum formed (***Table 25***). Compared to previous complex, second conformation leads to more red shifted transitions and it could be related with overlapping orbital between pyridine a metal is more hindered due they are not aligned. Even only one azide is in contact with picole, picole is aligned to metal in some way that facilitates a small back bonding character.

SOC contribution was also calculated leading to the most red-shifted transition at 443nm, that could explain activation of drug around (***Table 26***). May another configuration with picole not aligned and different azide orientation could give more red-shifted spectrum, thus also transitions.

IV.3.5 Comparison of the four complexes regarding photo-reactivity

Considering **7**, **8**, **9**, and **10** complexes have the same hydroxyl and azide ligands, a correlation is seen that increasing the pyridine based ligands, SOC contribution allows more blue-shifted transitions. It could be explained that more electron-withdrawing elements are put on cyclic ligands, adding an alkylating group as methyl on complex **10** or adding a new pyridine as amine ligand results on reducing electron density on platinum making the metal center more positive and inducing a bigger magnetic field which will apply a stronger torque force making easier to electron magnetic spin to change the direction. Aiming this complex **10** should have another conformation where SOC contribution increases and explains its experimental behavior as for three remaining complexes.

Experimentally, the four complexes present considerable phototoxicity against cisplatin-resistant cancer cell line, meaning a deferent approach of action. One reason could be that among photo-activated complex formed, also triplet states presence leads to a photodynamic therapy process. Studies have shown that platinum (II) with cyclometallating ligands present a promising photosensitizer that can be used on PDT.[46] In photodynamic therapy, photosensitizer molecule goes by non-radiative via intersystem crossing to a triplet state and transfer energy to the medium giving rise for singlet oxygen formation. Taking in consideration experimental results show that our complex system evolves to triplet states, therefore their enhanced activity could be related to the formation of singlet oxygen.

This double approach of activity of photo-activated complexes also overcome a throwback where singlet oxygen does not reach DNA directly, because singlet oxygen is short-lived in biological systems, presenting a short diffusion length. Due tumor areas are hypoxic; when the complex is activated after releasing one or all azide ligands, most commonly hydroxyl ligands are still present which increase the possibility of formation of reactive oxygen species(ROS) very close to DNA, due to availability of oxygen. Unfortunately, not experimental procedure has been used to prove the formation of singlet oxygen on discussed complexes.

Singlet oxygen ($^1O_2$) reacts with DNA; nitrogenous bases are oxidized due to their low redox potential. Lower redox potential is for guanine, becoming easier to go under oxidative stress and become 8-oxo-7,8-dihydro-20-deoxyguanosine (8-oxodG) which becomes more susceptible to oxidation in this form, until the formation of oxaluric acid. On single DNA it strand was proved that DNA polymerase is not able to pass through damaged guanines. Another way of damage to the cell is related to oxidation of guanine, leading to G to T transversions in a thymine tautomeric form. Different forms of damage are present due to singlet oxygen presence, aiming its high activity with biomolecules.[47] Even damage produced by this ROS species depends on short life of singlet oxygen, in this case presence of oxygen released by complexes leads to PDT approach due treatment is localized.

IV.4   Evaluation of potential biological activity: protein docking

The mechanism of action of these anticancer drugs is also defined by the interaction that it is establishing with DNA molecule. For all docking studies with all complexes, the DNA molecule was derived from 1BNA, which is a B-DNA structure obtained from protein data bank(PDB). DNA structure was slightly modified; at one side a guanine nitrogenous base was added in order to obtain

two adjacent guanines, and to the other extreme guanine it was also added to obtain two adjacent guanines.

To ensure a more realistic dock, a preliminary test was conducted with cisplatin, which is a well-studied complex. Cisplatin, $[Pt(NH_3)_2Cl_2]$, most commonly undergoes chlorine dissociation once it goes into the cell due to the extracellular higher chlorine concentration fulfilling Le Chatelier principle. Consequently, coordination positions can be occupied by water molecules, becoming a diaqua complex that will lead these two coordination sites to nitrogenous bases constituting DNA. Specifically, Cisplatin was docked between two adenine nitrogenous bases (*Figure 22*).
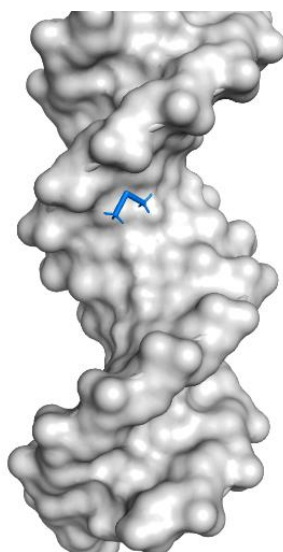

Figure 22 Cisplatin DNA docking

IV.4.1 Ligand lability based on the electronic properties of each complexes

Prior to the docking process, it is important to know if azide ligand could be released. Consequently, the complex would be optimized without the azide ligand. TDDFT calculation was carried out in order to make a qualitative study of which ligand is more prone to leave and reduce the metal after azide.

For complex **7**, after the release of one azide ligand it reaches a trigonal bipyramidal geometry. TDDFT calculation was carried out for this complex, showing that, above 280 nm, transitions tend to go to the LUMO orbital. LUMO orbital presents an important associative orbital at the platinum center with amine derived ligands involving a bonding part of hydroxyl and azide ligand as well. However, a strong dissociative character is seen on the other hydroxyl ligand due to its interaction with a double contact with the big, previously mentioned, bonding orbital and metal orbital in a dissociative

character. As a consequence, the hydroxyl ligand would be pretty clear to leave earlier, and remaining labile ligands will depend on the square-plane trans effect that will lead to dissociation of OH. Moreover, a small contribution also comes from transitions reaching LUMO+1 and LUMO+2 orbitals, which present an IL charge transfer and a strong dissociative character of azide and amine derived ligands, respectively.

Complex **8** presents a very similar behavior to the complex **7**, in which the major contribution from transitions lead to the LUMO orbital that also presents an important associative orbital involving amine derived ligands and surrounding platinum, leaving aside OH and N_3 bonds this time. In the same manner as the previous complex, a double contact dissociative character is seen on OH ligands facilitating their release. Additionally, azide has also a dissociative character with the platinum center but involving only one contact, making the interaction less intense than the double contact established by hydroxyl ligands.

For complex **9**, after azide release the compound reaches a distorted trigonal bipyramidal geometry. TDDFT calculation was also carried out to know which ligand could leave before the docking process. Wavelengths used for drug activation must be visible shifted, so most transitions above 300nm go to LUMO orbital which presents a solid associative character between amine derived ligands involving platinum, meaning a low possibility of pyridine release during irradiation. Moreover, a dissociative character between the remaining azide ligand N_3-Pt and hydroxyl ligand OH-Pt is present.

Hydroxyl antibonding orbital margin has two contacts, while a solid associative bonding with amine ligands mentioned above and the other clash with the metal orbital. Considering LUMO orbital, OH release could be explained, but there is still a dissociative character advantaging azide release that could be explained by the trans effect. Based on trans-effect, pyridine ligands are secured due to their backbonding that makes equal bonding interaction between Py-Pt bonds. Instead, the trans-effect is placed on the azide ligand, making OH a better leaving group. It is well-known that the trans effect of OH is minimal while azide ligand present a strong trans-effect. This effect origin from the presence of partially empty antibonding orbitals that contributes with pi-acceptor character making bonding interaction stronger while weakening the OH-Pt bond.

For complex **10**, above 300nm major contributions come from transitions originating from different HOMO bonding orbitals to the LUMO orbital, which possess the same character as in complex **9**. Hence, the same behavior of previously discussed complexes is observed even though a methyl is

present on the pyridine ligand. Methyl in picole is not directly bonded to the positions 2 and 6 where it would be the most influential on pi acceptor character. So, its character is not equal but similar to the bi-pyridine complex.

Based on the previous discussion on ligands release in each complex, and which form they can adopt, the docking process was carried out for each one.

IV.4.2 Protein docking

For complex **7**, first a big grid box was tested comprised of the whole DNA part, then was tested a small and punctual grid box. The following dock, in which the complex is located between adenine and guanine nitrogenous bases, was obtained. Platinum is 2.5 Å away from N7-guanine and 3.5 Å away from N7-adenine, so there are two possible nucleophilic attacks from purines N7 position. Nevertheless, the platinum center is closer to the N7 of guanine unit (*Figure 23*). Additionally, there is the possibility that hydrogen bond formed with adenine and azide-7N (adenine) drag the positive center towards its site, increasing the possibility to coordinate with adenine nitrogenous base.
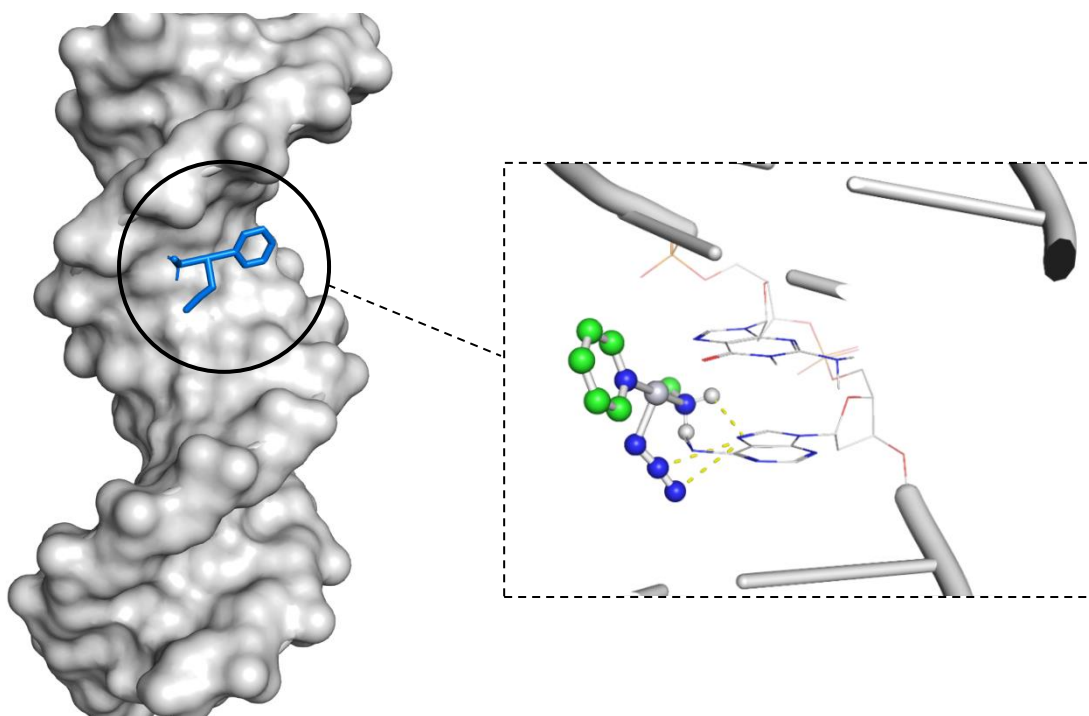

Figure 23 Complex 7 docking to DNA.

For a better understanding, QM calculation was carried out using only two nitrogenous bases because of the expensive character of these calculations if more bases are included. Results of QM computation gives the coordination of platinum center with N7 of guanine, ending at a 2 Å distance that is similar

to other coordination lengths (*Figure 24*). After coordination, adenine has been displaced from its original position locally altering the form of DNA. Platinum monoadduct formed with guanine presents a square planar geometry that is favored for platinum(II) species. Because the process is continually under irradiation, loss of azide ligand could be achieved but there would be a competence of stability between forming a bifunctional adduct or with remaining azide or NH_3(azide derived) ligand. It was experimentally reported that the greater product was the mono-adduct one, followed by bifunctional adduct of complex with 5´-GMP, which is present freely without a steric character of bases present around. Due adduct results are obtained from H NMR based on a previously reported photoactive complex, bond distances could not be obtained only adduct forms. In this case, it is more probable not to see a considerable amount of interstrand or intrastrand crosslinks due to the steric hindrance generated by the anticancer drug. This theory also could be correlated to cisplatin, a platinum-based drug that form bifunctional adducts quickly while transplatin does not present this ability to form bifunctional adducts in DNA. [48]
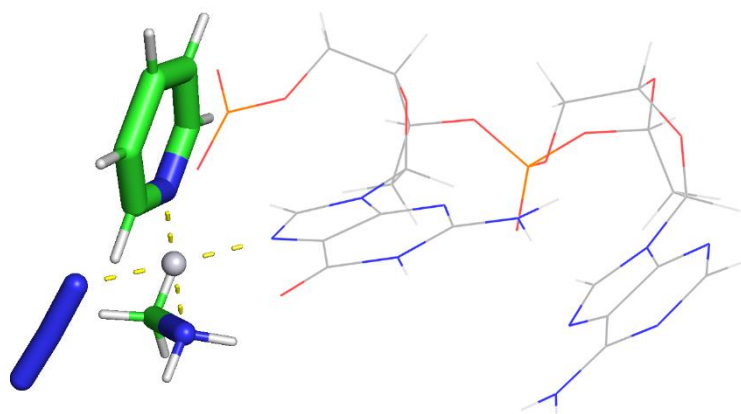

Figure 24 QM of complex 7

For complex **8**, dock with a small grid box resulted in the interaction of N-thiazole with N7-guanine and azide nitrogenous with N7-adenine (*Figure 25*). QM was also performed on the active site to achieve a better definition of the docking at this site.
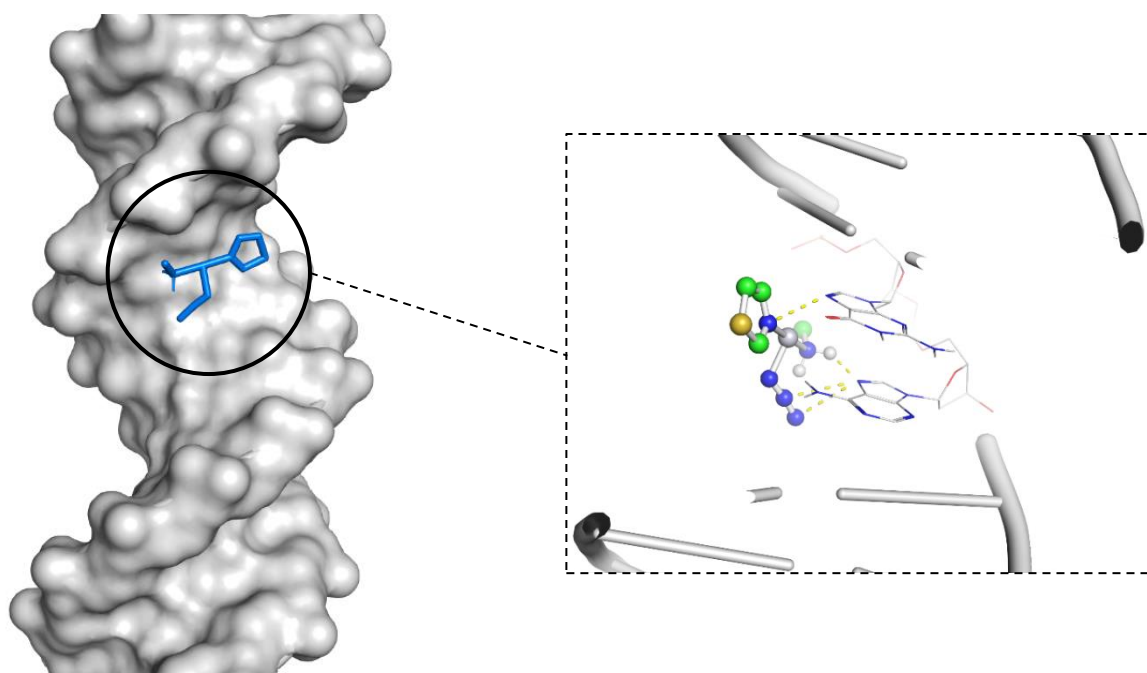
Figure 25 Complex 8 dock to DNA

QM part of the complex 8 present a similar behavior as the complex 7, which coordinates to N7-guanine (*Figure 26*). Hypothetically, these two complexes with only one cyclic ligand could be more related than bi N-cyclic ligands complexes to bifunction al adducts due to less steric hindrance with the bases.
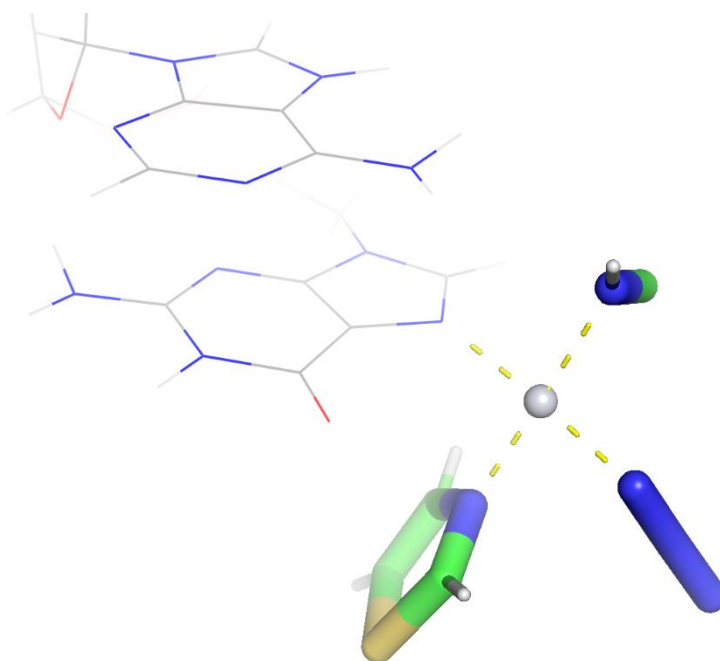
Figure 26 QM of complex 8.

For complex **9**, the docking result is presented on *Figure 27,* in which azide ligand interacts with two adjacent adenine of A strand and is very close to adenine and adjacent thymine of B strand. In the same manner, QM method was used in order to find the exact localization of the docking of this complex.
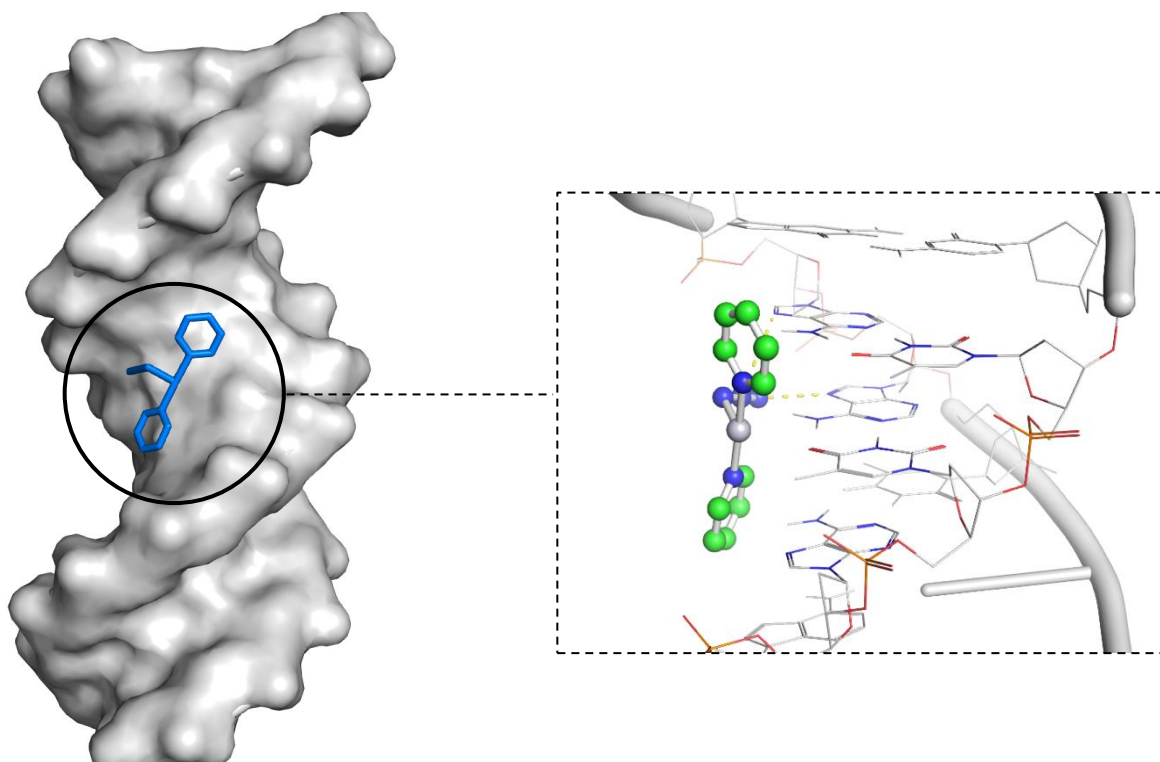

Figure 27 Complex 9 dock to DNA

QM calculation were carried out establishing two boxes, a big which includes four nitrogenous bases (*Figure 28*) and a small box where only one possible coordination nitrogenous base is included (*Figure 29*). Taking into account that QM calculations for 4 nitrogenous bases could take a longer time it will be used to define a distance between two possible nucleophilic attacks taking in consideration steric hindrance that pyridine ligands represent. Taking the ultimate iteration without convergence, the distances between platinum center with oxygen (Thymine) and Nitrogen (adenine) were 3 and 3.3 Å, respectively.
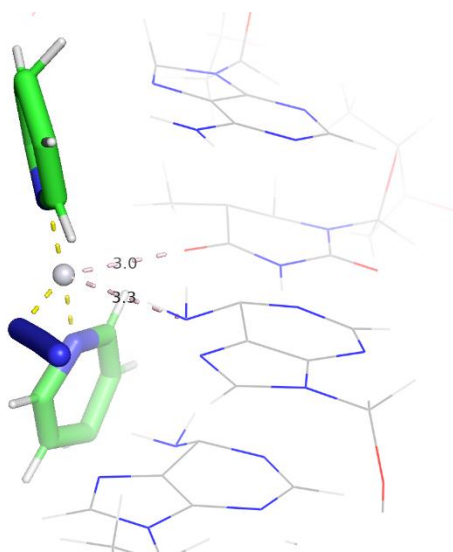

Figure 28 Big box QM for complex 9.

On small box docking using QM (*Figure 29*), a closer interaction is achieved to platinum due it is a less expensive calculation and not inherence of adjacent nitrogenous bases is counted. Final distance formed between platinum and oxygen from thymine reaches 2.1 Å, being coordinated in this way to DNA. A special feature of these complex is its enhanced activity, which not only seems to depend on the platinum but also on the interaction between pyridine ligand with adjacent nitrogenous bases, assuring a stronger binding force of this docking. In fact, pyridine interaction is governed by electrostatic interactions between the negative charges, present on oxygen or nitrogen of nitrogenous bases, with the positive charges of pyridines hydrogen. Furthermore, the possible resonant structures of pyridine favor the appearance of local charges that could enhance the electrostatic interactions between pyridine and DNA.
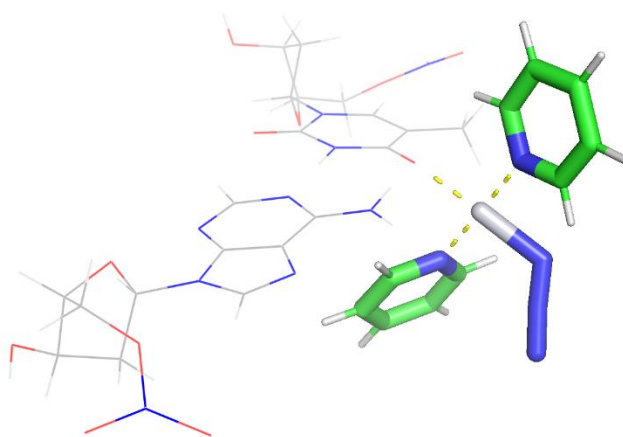
UNIVERSIDAD
YACHAY
TECH

SCHOOL OF
CHEMICAL SCIENCES
AND ENGINEERING

Figure 29 Small box QM for complex 9.

For complex **10**, docking results show interactions between azide ligand and two adjacent N7-adenine nitrogenous bases (*Figure 30*). Platinum center is placed between thymine and adenine.
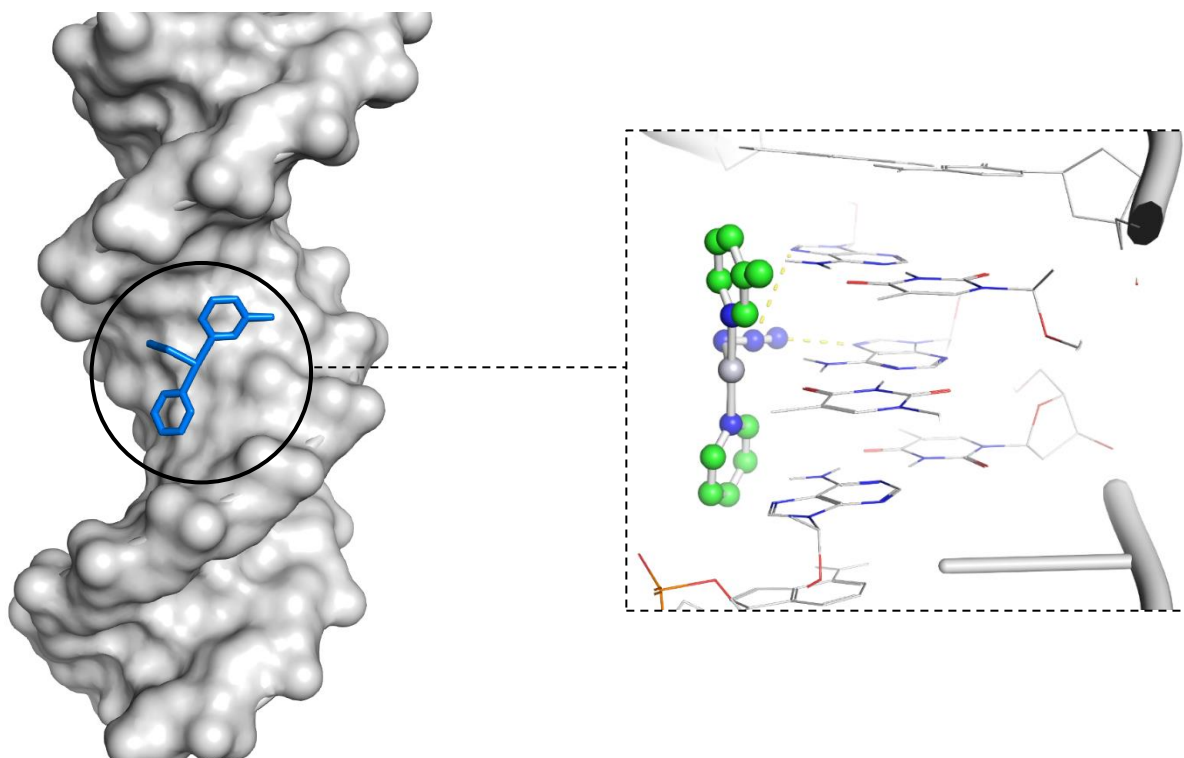

Figure 30 Complex 10 dock to DNA

The docking of the complex **10** results in a very similar position to the one reached by the complex 9. For QM calculations, a small box with two nitrogenous bases was constructed giving as a result a docking with oxygen pertaining to the thymine. This results could be related to the steric factor that nitrogen, and its subsequent bonded hydrogen atoms, of adenine represents preventing a strong interaction with the complex. Distance between platinum center and oxygen is about 2.1 Å, the same distance established by complex 8 with the same oxygen (*Figure 31*).
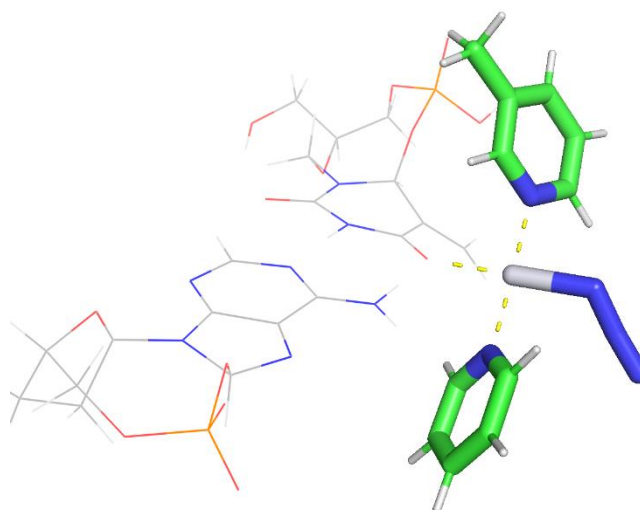

Figure 31 QM for complex 10.

Complexes **7** and **8** have a cyclic bulky ligand which does not release when it binds to DNA, therefore it could show as a stop signal to RNA polymerase. Complexes **9** and **10** dock results show that drug is placed in the middle of the double strand DNA, in which their cyclic amine derived ligands interact with opposite nitrogenous bases that could lead to the stop of DNA Helicase meaning another mechanism of action due its enhanced activity ergo overcoming resistance problem.

Chapter V   Conclusions

- Singlet and triplet bond distances formed by platinum were determined, indicating that triplet state present azide-platinum bond elongation for complex **7**, **8**, **9** and **10**, intrinsically related to dismissing platinum charge. Dismiss on charge is related to the reduction of Mulliken positive charge from singlet to triplet states. This effect leads to that an easier possibility to give one electron to metal in order to reduce it, as observed with azide making easier to achieve the active complex. Instead of it, **8.1** and **9.2** do not present this character due they present amine derived elongation which is not seen experimentally.

- From DFT and TDDFT calculations, HOMO and LUMO orbitals of all complexes were drawn. All of them present a similar character on the LUMO orbital corresponding to a strong antibonding character between platinum and azide ligand, while a weak dissociative character between platinum and hydroxyl or amine derived ligands was observed. For any transition going from any HOMO to LUMO orbital will present a small band gap energy corresponding to azide release, making more possible an activation at longer wavelengths leading to promising complexes.

- TDDFT and SOC contribution were calculated for each conformation. As we observed, if amine derived ligands are less aligned it would influence more the back bonding character, leading to a smaller octahedral splitting. Consequently, more visible transitions are possible to achieve drug photo-activation. However, even if SOC contribution allows in these complexes transition at higher wavelengths, the experimental activation wavelength was not reached for complex **10**. However, considering errors present at DFT, such as self-interaction error, a reasonable agreement was found. Additionally, more conformations could have been taken into account inducing different orbital overlap.

- SOC contribution has been presented to increase from complex **7** to complex **10**, that is related to more substituted amine derived ligands. More electron withdrawing elements on amine derived complex, makes platinum center more positive forming a stronger magnetic field so making easier for the electron to change its spin direction and to reach a triplet state.

- Docking computation for active complex of each complex were carried out. It is well known that nucleophilic attack of N7- adenine or N7-guanine is likely to coordinate to platinum. After docking results, complexes 7 and 8 showed a strong interaction with N7-guanine. On the other hand, complexes 9 and 10 do not show such coordination to N7-guanine but rather a bond to the oxygen of thymine. In addition, the interaction between cyclic ligands and adjacent

nitrogenous bases suggest a different mechanism of action and thus it would be necessary to overcome target and resistance problems.

Recommendation

As a general recommendation, developing of a theoretical study before synthesizing could provide a better understanding of mechanism of drug, drug activation, and less trial fail processes to get a complex that could be activated at longer wavelength.

Chapter VI Bibliography

1. Organization, W. H. Cancer. https://www.who.int/news-room/fact-sheets/detail/cancer (2018).

2. American Cancer Society. Cancer Basics: What is cancer? *Am. Cancer Soc.* 1–7 (2015).

3. Sudhakar, A. History of Cancer, Ancient and Modern Treatment Methods. *J. Cancer Sci. Ther.* **01**, (2009).

4. Arruebo, M. *et al.* Assessment of the evolution of cancer treatment therapies. *Cancers* vol. 3 (2011).

5. Ndagi, U., Mhlongo, N. & Soliman, M. E. Metal complexes in cancer therapy – An update from drug design perspective. *Drug Design, Development and Therapy* vol. 11 (2017).

6. Farrer, N. J., Salassa, L. & Sadler, P. J. Photoactivated chemotherapy (PACT): The potential of excited-state d-block metals in medicine. *Dalt. Trans.* (2009) doi:10.1039/b917753a.

7. Johnstone, T. C., Suntharalingam, K. & Lippard, S. J. The Next Generation of Platinum Drugs: Targeted Pt(II) Agents, Nanoparticle Delivery, and Pt(IV) Prodrugs. *Chemical Reviews* vol. 116 (2016).

8. Kratochwil, N. A., Bednarski, P. J., Mrozek, H., Vogler, A. & Nagle, J. K. Photolysis of an iodoplatinum(IV) diamine complex to cytotoxic species by visible light. *Anticancer. Drug Des.* **11**, (1996).

9. Lemma, K., Berglund, J., Farrell, N. & Elding, L. I. Kinetics and mechanism for reduction of anticancer-active tetrachloroam(m)ine platinum(IV) compounds by glutathione. *J. Biol. Inorg. Chem.* **5**, (2000).

10. Bednarski, P. J. *et al.* Light-activated destruction of cancer cell nuclei by platinum diazide complexes. *Chem. Biol.* **13**, (2006).

11. Shi, H., Imberti, C. & Sadler, P. J. Diazido platinum(IV) complexes for photoactIVated anticancer chemotherapy. *Inorganic Chemistry Frontiers* vol. 6 (2019).

12. Imran, M., Ayub, W., Butler, I. S. & Zia-ur-Rehman. Photoactivated platinum-based anticancer drugs. *Coord. Chem. Rev.* **376**, 405–429 (2018).

13. Szaciłowski, K., Macyk, W., Drzewiecka-Matuszek, A., Brindell, M. & Stochel, G. Bioinorganic photochemistry: Frontiers and mechanisms. *Chemical Reviews* vol. 105 (2005).

14. Ash, C., Dubec, M., Donne, K. & Bashford, T. Effect of wavelength and beam width on penetration in light-tissue interaction using computational methods. *Lasers Med. Sci.* **32**,

(2017).

15. D'Andrea, A. D. DNA Repair Pathways and Human Cancer. in *The Molecular Basis of Cancer: Fourth Edition* (2014). doi:10.1016/B978-1-4557-4066-6.00004-4.

16. Wang, Z. & Zhu, G. DNA Damage Repair Pathways and Repair of Cisplatin-Induced DNA Damage. in *Reference Module in Chemistry, Molecular Sciences and Chemical Engineering* (Elsevier, 2018). doi:10.1016/b978-0-12-409547-2.14251-9.

17. Huang, Y. & Li, L. DNA crosslinking damage and cancer - a tale of friend and foe. *Translational Cancer Research* vol. 2 (2013).

18. Photochemical and Photobiological Reviews. Kendric C. Smith . *Q. Rev. Biol.* **55**, (1980).

19. Klaunig, J. E. & Kamendulis, L. M. 3.09 Carcinogenicity. **2**, 121–132 (2010).

20. Harper, B. W. *et al.* Advances in platinum chemotherapeutics. *Chemistry - A European Journal* vol. 16 (2010).

21. Han, X., Sun, J., Wang, Y. & He, Z. Recent Advances in Platinum (IV) Complex-Based Delivery Systems to Improve Platinum (II) Anticancer Therapy. *Med. Res. Rev.* **35**, (2015).

22. Mitra, K. Correction: Platinum complexes as light promoted anticancer agents: a redefined strategy for controlled activation. *Dalt. Trans.* **46**, (2017).

23. Vogler, A., Hüttermann, J. & Fußeder, B. Photochemical Reductive trails-Elimination from Jrcms-Diacidotetracyanoplatinate(IV) Complexes. *Zeitschrift fur Naturforsch. - Sect. B J. Chem. Sci.* **33**, (1978).

24. Šima, J. Photochemistry of azide-moiety containing inorganic compounds. *Coordination Chemistry Reviews* vol. 250 (2006).

25. Vogler, A. & Hlavatsch, J. Photochemical Four-Electron Redox Reaction of Hexaazidoplatinate(IV). *Angew. Chemie Int. Ed. English* **22**, (1983).

26. Müller, P. *et al.* Nucleotide cross-linking induced by photoreactions of platinum(IV)-azide complexes. *Angew. Chemie - Int. Ed.* **42**, (2003).

27. Hall, M. D. & Hambley, T. W. Platinum(IV) antitumour compounds: Their bioinorganic chemistry. *Coordination Chemistry Reviews* vol. 232 (2002).

28. Mackay, F. S. *et al.* A photoactivated trans-diammine platinum complex as cytotoxic as cisplatin. *Chem. - A Eur. J.* **12**, (2006).

29. Westendorf, A. F. *et al.* Trans,trans,trans-[PtIV(N3)2(OH) 2(py)(NH3)]: A light-activated antitumor platinum complex that kills human cancer cells by an apoptosis-independent mechanism. *Mol. Cancer Ther.* (2012) doi:10.1158/1535-7163.MCT-11-0959.

30. Westendorf, A. F. *et al.* Influence of pyridine versus piperidine ligands on the chemical, DNA binding and cytotoxic properties of light activated trans,trans,trans-[Pt(N 3)2(OH)2(NH3)(L)]. *J. Inorg. Biochem.* (2011) doi:10.1016/j.jinorgbio.2011.01.003.

31. MacKay, F. S. *et al.* Synthesis, characterisation and photochemistry of PtIV pyridyl azido acetato complexes. *Dalt. Trans.* (2009) doi:10.1039/b820550g.

32. Zhao, Y. *et al.* Diazido mixed-amine platinum(IV) anticancer complexes activatable by visible-light form novel DNA adducts. *Chem. - A Eur. J.* (2013) doi:10.1002/chem.201300374.

33. Farrer, N. J. *et al.* A potent trans-diimine platinum anticancer complex photoactivated by visible light. *Angew. Chemie - Int. Ed.* (2010) doi:10.1002/anie.201003399.

34. *IUPAC Compendium of Chemical Terminology*. *IUPAC Compendium of Chemical Terminology* (2009). doi:10.1351/goldbook.

35. Kauffman, G. B. Inorganic Chemistry, 2nd Edition (Miessler, Gary L.; Tarr, Donald A.). *J. Chem. Educ.* (2000) doi:10.1021/ed077p165.1.

36. Shaili, E. *et al.* Platinum(iv) dihydroxido diazido: N-(heterocyclic)imine complexes are potently photocytotoxic when irradiated with visible light. *Chem. Sci.* **10**, (2019).

37. Neese, F. The ORCA program system. *Wiley Interdiscip. Rev. Comput. Mol. Sci.* **2**, (2012).

38. Younker, J. M. & Dobbs, K. D. Correlating experimental photophysical properties of iridium(III) complexes to spin-orbit coupled TDDFT predictions. *J. Phys. Chem. C* **117**, (2013).

39. Hanwell, M. D. *et al.* Avogadro: An advanced semantic chemical editor, visualization, and analysis platform. *J. Cheminform.* (2012) doi:10.1186/1758-2946-4-17.

40. Perdew, J. P., Burke, K. & Ernzerhof, M. Generalized gradient approximation made simple. *Phys. Rev. Lett.* **77**, (1996).

41. ORCA Input Library. Basis sets. https://sites.google.com/site/orcainputlibrary/basis-sets.

42. Neese, F. *et al.* Orca 4.0.1. *Wiley Interdiscip. Rev. Comput. Mol. Sci.* **2**, 73–78 (2012).

43. Library, O. I. Geometry optimizations. https://sites.google.com/site/orcainputlibrary/geometry-optimizations.

44. Morris G.M. & Dallakyan S. AutoDock — AutoDock. *02-27* **1**, 15–45 (2013).

45. Majumdar, S., Majumdar, H. S., Österbacka, R. & McCarthy, E. Organic Spintronics. in *Reference Module in Materials Science and Materials Engineering* (2016). doi:10.1016/b978-0-12-803581-8.00577-4.

46. Doherty, R. E. *et al.* Photodynamic killing of cancer cells by a Platinum(II) complex with cyclometallating ligand. *Sci. Rep.* **6**, (2016).

47. Agnez-Lima, L. F. *et al.* DNA damage by singlet oxygen and cellular protective mechanisms. *Mutat. Res. - Rev. Mutat. Res.* **751**, 15–28 (2012).

48. Weber, G. F. & Weber, G. F. DNA Damaging Drugs. in *Molecular Therapies of Cancer* (2015). doi:10.1007/978-3-319-13278-5_2.